Nirmal Gwalior

TECHNOLOGY INNOVATION AND INCUBATION CENTER (TIIC)
Atal Bihari Vajpayee – Indian Institute of Information Technology & Management (ABV-IIITM), Gwalior
(An Autonomous Institute of National Importance, Government of India)

PROJECT REPORT
AI-ENABLED CONSTRUCTION & DEMOLITION (C&D) WASTE MANAGEMENT SYSTEM FOR GWALIOR SMART CITY

Submitted By
LORD-TECH DATUS SOLUTIONS PRIVATE LIMITED

Principal Investigator (PI)
- Dr. Kamal Sharma (Director, Lord-Tech Datus Solutions Private Limited)

Co-Principal Investigators (Co-PIs)
- Mr. Manish Bharadwaj
- Mr. Amal Bajpai

Incubated Under
Technology Innovation and Incubation Center (TIIC)
TIDE 2.0 Scheme

Financial Support
Grant-in-Aid: ₹2,00,000 (Rupees Two Lakhs Only)

Project Duration
October 2025 – October 2026

Submitted To
Technology Innovation and Incubation Center (TIIC)
Atal Bihari Vajpayee – Indian Institute of Information Technology & Management (ABV-IIITM), Gwalior

Abstract

Construction and demolition (C&D) waste management is essential for sustainable urban development because conventional inspection methods are labor-intensive, subjective, and incapable of providing rapid material quantification and environmental impact assessment. This study presents an artificial intelligence (AI)-driven framework for automated C&D waste analysis using manually collected field images from Gwalior Smart City, India. A dataset comprising 506 labeled images across five material categories (brick, concrete, soil, steel, and wood) was developed and used to train a multi-task pipeline integrating DenseNet121 with Transformer encoders for material classification, LayerCAM-assisted weakly supervised U-Net segmentation, monocular depth estimation using MiDaS, and three-dimensional volume reconstruction. The estimated material volumes were subsequently employed to quantify waste mass and CO_2 emissions through material-specific emission factors. The proposed classification model achieved an overall accuracy of 87.25%, weighted F1-score of 0.8730, and micro-average AUC of 0.9674, demonstrating reliable recognition of diverse C&D materials. The segmentation model obtained a validation Dice coefficient of 0.6097 and mean Intersection-over-Union (IoU) of 0.3396, enabling effective region delineation without manual pixel-level annotations. Volume-based environmental assessment estimated a total CO_2 emission of 367.45 tonnes for the test dataset, highlighting the dominant contribution of steel waste while accounting for the carbon-sequestering effect of wood. The proposed framework integrates classification, segmentation, depth estimation, and carbon accounting into a single deployable workflow suitable for smartphone-based field applications. The results demonstrate the potential of AI-enabled C&D waste analytics to support smart-city monitoring, improve waste recycling strategies, and facilitate data-driven environmental decision-making for sustainable urban infrastructure.

TABLE OF CONTENTS

LIST OF FIGURES

LIST OF TABLES

1. Introduction

Rapid urbanization, infrastructure expansion, and building redevelopment have substantially increased the generation of construction and demolition (C&D) waste worldwide. C&D waste constitutes one of the largest solid waste streams, accounting for approximately one-third of all waste generated in many countries, and its improper disposal contributes to landfill depletion, greenhouse gas emissions, resource depletion, and environmental degradation. Sustainable management of C&D waste has therefore become a strategic priority for governments and smart cities seeking to achieve circular economy objectives, improve resource efficiency, and reduce the environmental footprint of the construction sector. Effective segregation and quantification of reusable materials such as concrete, brick, steel, wood, and soil are essential for maximizing recycling rates and minimizing disposal costs (Cheng et al., 2024; Lu et al., 2023).

Traditional C&D waste monitoring largely depends on manual inspection, visual estimation, and laboratory-based material characterization. These approaches are labor-intensive, time-consuming, subjective, and unsuitable for real-time monitoring of large-scale construction sites. Moreover, manual estimation often fails to provide accurate information regarding material composition, waste volume, or associated carbon emissions, thereby limiting its usefulness for sustainable planning and policy implementation. The emergence of Industry 4.0 technologies, particularly artificial intelligence (AI), computer vision, unmanned aerial systems, and Internet of Things (IoT)-based sensing, has created new opportunities for automating waste identification and improving environmental decision-making through data-driven analytics (Akinade & Oyedele, 2019; Wang et al., 2023).

Deep learning has demonstrated remarkable success in visual recognition tasks involving complex construction environments. Convolutional Neural Networks (CNNs), including DenseNet, ResNet, EfficientNet, and Vision Transformers (ViTs), have significantly improved object recognition by learning hierarchical texture and structural features directly from images. Hybrid CNN–Transformer architectures further enhance performance by combining local feature extraction with global contextual reasoning, making them particularly suitable for heterogeneous C&D waste containing multiple material textures and varying illumination conditions. These models consistently outperform conventional machine learning approaches in classification accuracy and robustness under challenging field conditions (L. A. Akanbi et al., 2018; Akinade et al., 2017).

Beyond material classification, semantic segmentation enables pixel-level localization of waste components, allowing accurate estimation of individual material regions. However, the development of supervised segmentation models generally requires large quantities of manually annotated masks, which are expensive and time-consuming to produce for construction environments. Weakly supervised learning techniques such as LayerCAM provide an effective alternative by generating pseudo-labels from image-level annotations, thereby substantially reducing annotation effort while preserving satisfactory localization accuracy. Combined with encoder–decoder architectures such as U-Net, weakly supervised segmentation has become an attractive solution for practical construction waste applications where dense annotations are unavailable (J. Chen et al., 2021; Etim, 2024).

Recent advances in monocular depth estimation have further expanded the capabilities of computer vision systems beyond two-dimensional image analysis. Models such as MiDaS estimate dense depth information from a single RGB image, enabling three-dimensional reconstruction of objects without specialized depth sensors. Integrating depth estimation with semantic segmentation allows estimation of material volume and waste mass directly from smartphone images, facilitating quantitative assessment of construction debris in field conditions. Such capabilities provide an economical alternative to LiDAR or stereo imaging systems while supporting rapid deployment in smart-city applications (Lu et al., 2015).

In parallel with waste quantification, environmental sustainability has become a major concern in the construction industry due to its significant contribution to global carbon emissions. Accurate estimation of embodied CO_2 emissions associated with different waste materials enables authorities to evaluate recycling benefits, prioritize resource recovery, and support low-carbon construction policies. Existing AI-based waste classification studies primarily focus on recognition accuracy, whereas relatively few integrate automated material identification with volumetric reconstruction and carbon accounting within a unified framework. Consequently, practical tools capable of simultaneously identifying waste materials, estimating their spatial extent, reconstructing three-dimensional volume, and quantifying environmental impacts remain limited (Lee et al., 2016).

To address these challenges, this study proposes an integrated AI-driven framework for smart C&D waste management using manually collected field images from Gwalior Smart City, India. The proposed system combines a DenseNet121–Transformer classification network, LayerCAM-assisted weakly supervised U-Net segmentation, MiDaS-based monocular depth estimation, and volume-based CO_2 emission quantification into a unified pipeline. The framework is designed to automatically classify five major C&D material categories, reconstruct material volumes from single RGB images, estimate waste mass and carbon emissions, and generate deployable outputs suitable for smartphone-assisted field inspection.

By integrating classification, segmentation, depth estimation, and environmental assessment into a single workflow, the proposed approach contributes toward intelligent waste monitoring systems that support circular economy practices and sustainable urban infrastructure management. The methodology and experimental results presented in this study demonstrate the feasibility of AI-enabled environmental analytics for next-generation smart-city waste management.

2. Objectives

Objectives of the project are given as follows;

1. Design and train a multi-task deep learning pipeline for material classification, segmentation, and volumetric estimation.
2. Build a manually curated, city-specific image dataset covering five C&D material classes.
3. Integrate depth estimation (MiDaS or gradient fallback) with segmentation masks for 3-D volume reconstruction.
4. Develop a CO_2 emission calculator using volume-based emission factors.
5. Produce a deployable single-image inference pipeline suitable for field officers with a smartphone.

3. Methodology

3.1 Dataset Description

The dataset used in this study consisted of manually collected field images of construction and demolition waste from Gwalior, Madhya Pradesh, India. The images were categorized into five major C&D waste material classes: brick, concrete, soil, steel, and wood. A total of 506 labelled images were compiled and used for model development and evaluation. The dataset was divided into training, validation, and testing subsets using a stratified splitting approach to preserve class balance across all material categories. The final dataset distribution included 202 images for training, 202 images for validation, and 102 images for testing, corresponding to 39.9%, 39.9%, and 20.2% of the total dataset, respectively (J. Li et al., 2022; Luga et al., 2025). The computational environment and major software libraries used for model training, image preprocessing, segmentation, depth estimation, and visualization are summarized in Table 1.

Table 1. Hardware and Software Requirements:

Component	Specification
Compute platform	Google Colab Pro (T4/A100 GPU, 12–40 GB VRAM)
Python version	3.10
Deep learning fw.	TensorFlow 2.x / Keras functional API
Depth estimation	PyTorch + torch.hub (intel-isl/MiDaS, small)
Image processing	OpenCV 4.x, scikit-image, Pillow
Data science	NumPy, Pandas, scikit-learn
Visualisation	Matplotlib 3.x, Seaborn
Storage	Google Drive (/content/drive/MyDrive/cdw/)
Random seed	42 (all train_test_split calls)
Mixed precision	Not explicitly enabled; TF auto-cast on A100

The complete dataset contained a reasonably balanced distribution across the five material categories. Soil represented the largest share with 116 images, followed by wood with 104 images, concrete with 102 images, steel with 97 images, and brick with 87 images, as shown in Table 2.

Table 2. Train–validation–test split of the dataset

Dataset Split	Number of Samples	Percentage (%)
Training	202	39.9
Validation	202	39.9
Test	102	20.2
Total	**506**	**100.0**

The dataset was divided into training, validation, and testing subsets, as presented in Table 3. The split ensured that each subset retained a comparable class distribution, thereby reducing the risk of class imbalance during model training and evaluation.

Table 3. Class wise Distribution:

Class	Training (n=202)	Validation (n=202)	Test (n=102)
Brick	35 (17.3%)	35 (17.3%)	17 (16.7%)

Concrete	40 (19.8%)	41 (20.3%)	21 (20.6%)
Soil	47 (23.3%)	46 (22.8%)	23 (22.5%)
Steel	38 (18.8%)	39 (19.3%)	20 (19.6%)
Wood	42 (20.8%)	41 (20.3%)	21 (20.6%)
Total	**202 (100%)**	**202 (100%)**	**102 (100%)**

3.2 Image Preprocessing Pipeline

Before model training, all raw field images were subjected to a deterministic preprocessing pipeline to ensure uniform input quality and dimensional consistency. First, images were converted from BGR to RGB colour format using OpenCV. Each image was then resized to 224 × 224 pixels using INTER_AREA interpolation, which is suitable for downscaling because it reduces aliasing by averaging neighbouring pixel regions (Lu & Tam, 2013). To reduce sensor noise while preserving the texture characteristics of C&D waste materials, non-local means denoising was applied using cv2.fastNlMeansDenoisingColored with h = 5, hColor = 5, templateWindowSize = 7, and search Window Size = 21. Finally, pixel values were normalised by dividing by 255.0, converting all images into floating-point arrays within the range [0, 1] before being supplied to the neural network models.

To improve generalisation and reduce overfitting, data augmentation was applied only to the training subset. One augmented copy was generated for each training image, thereby synthetically expanding the training data while preserving the original validation and test sets for unbiased evaluation. The augmentation operations were implemented using the Keras ImageDataGenerator, as summarized in Table 4.

Table 4. Data augmentation parameters

Augmentation	**Range / Mode**	**Rationale**
Rotation	±25°	Simulates varied camera angles on-site
Width shift	±15%	Handles off-centre waste piles
Height shift	±15%	Accounts for camera tilt
Shear	±15°	Perspective distortion from oblique capture
Zoom	±20%	Variable capture distances (1–5 m)
Horizontal flip	0.5 prob.	Materials are laterally symmetric
Brightness jitter	0.8–1.2×	Lighting variability across field sessions

3.3 Material Classification Model Architecture: DenseNet121 + Transformer + Custom Head

The proposed material classification model was developed using a hybrid DenseNet121–Transformer architecture with a custom classification head, as illustrated in Figure 1. DenseNet121 was selected as the convolutional backbone because its dense connectivity pattern supports feature reuse and preserves fine-grained texture information, which is essential for distinguishing visually similar C&D waste materials such as brick, concrete, soil, steel, and wood (Cha et al., 2022; Hu et al., 2021). The backbone was initialized with ImageNet-1K pre-trained weights to improve feature extraction efficiency and reduce training instability on the relatively small field-image dataset.

The input image of size 224 × 224 × 3 is first passed through the DenseNet121 backbone, producing a final convolutional feature map of size 7 × 7 × 1024. During the initial training stage, the first N−100 layers of DenseNet121 were frozen to preserve generic visual representations, while the later layers were allowed to adapt to C&D material-specific textures. The resulting feature map was reshaped into 49 spatial tokens, each with 1024 feature dimensions, and learnable positional embeddings were added to retain spatial information before Transformer-based processing.

The Transformer component consisted of two sequential encoder blocks. Each block included multi-head self-attention with 8 attention heads, a key dimension of 64, residual connections, layer normalization, and a feed-forward network using GELU activation with dropout of 0.2 (Kang et al., 2022). This design enabled the model to capture long-range spatial relationships among waste material regions that may not be fully represented by convolutional operations alone.

After Transformer encoding, Global Average Pooling 1D was applied to convert the token sequence into a compact 1024-dimensional feature vector. This vector was then passed through a custom classification head containing three fully connected layers with 512, 256, and 128 neurons, respectively (Lakhouit, 2025). Each dense layer was followed by Batch Normalization, ReLU activation, and dropout rates of 0.5, 0.4, and 0.3. Finally, a Dense layer with Softmax activation generated class probabilities for the five target material categories: brick, concrete, soil, steel, and wood.

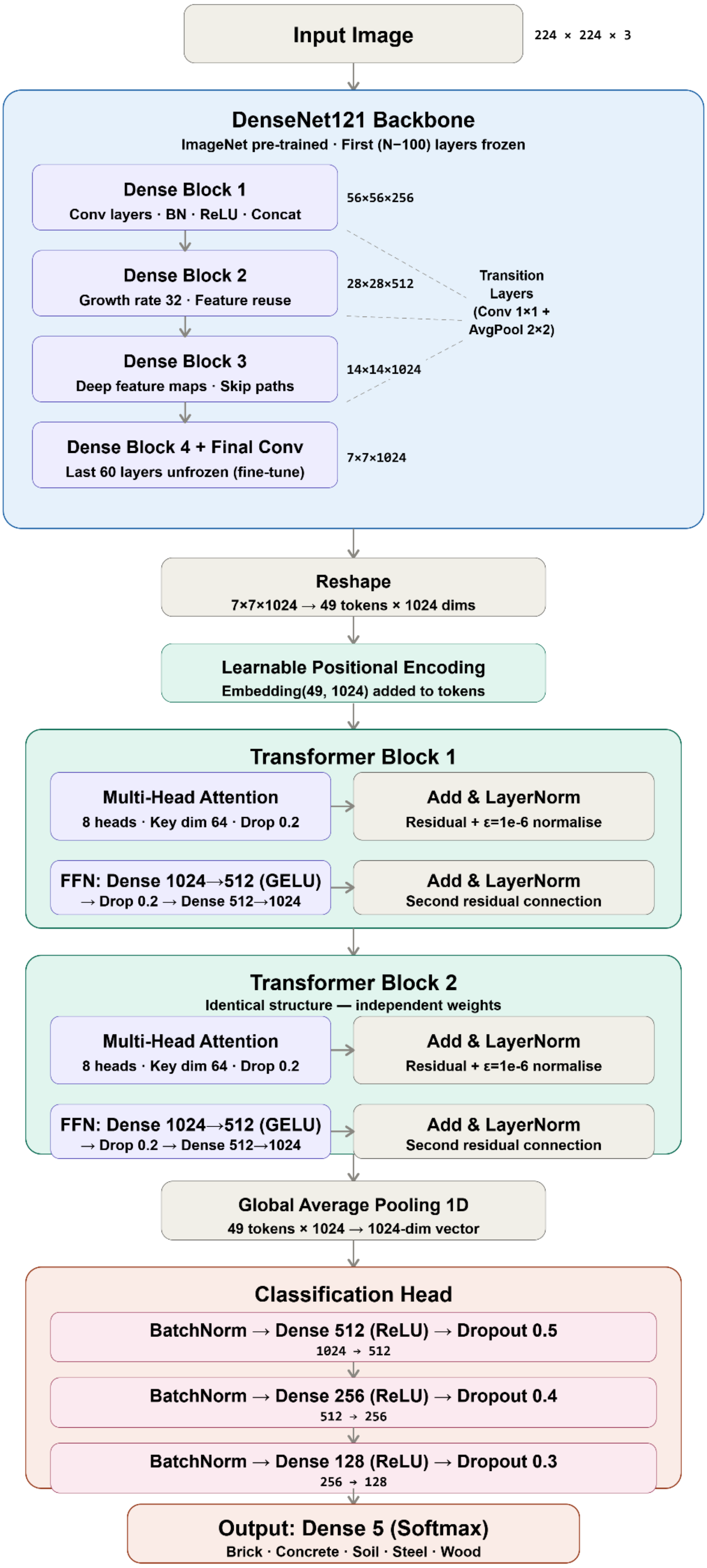

Figure 1. Classification Model Architecture

Table 5. Training Parameters

Hyperparameter	Value / Description
Input resolution	224 × 224 × 3 (RGB)
Batch size	32
Initial training epochs	30 (EarlyStopping patience=7)
Fine-tuning epochs	30 (EarlyStopping patience=5)
Initial LR	3×10^{-4} (Adam)
Fine-tuning LR	1×10^{-5} (Adam)
Loss function	Categorical Cross-Entropy (label smooth 0.1)
Frozen layers (initial)	First (N−100) DenseNet layers frozen
Unfrozen layers (fine-tune)	Last 60 DenseNet layers + full head
LR schedule	ReduceLROnPlateau (factor 0.3, patience 3)
Model checkpoint	Best val_accuracy (H5 format)

The classification model was trained using a two-stage transfer learning strategy. In the first stage, the early DenseNet121 layers were frozen, and only the later backbone layers, Transformer encoder, and classification head were trained using the Adam optimizer with a learning rate of 3×10^{-4}. In the second stage, the last 60 DenseNet121 layers were unfrozen and fine-tuned with the Transformer and classification head at a lower learning rate of 1×10^{-5}. This approach allowed the model to first learn stable high-level representations and then adapt the deeper convolutional features to the specific texture patterns of C&D waste materials. Early stopping, learning rate reduction on plateau, and model checkpointing were used to reduce overfitting and retain the best-performing model (Lin et al., 2023; Lu, 2019).

Model performance was evaluated using overall accuracy, macro and weighted precision, recall, and F1-score, along with one-versus-rest ROC-AUC, micro-average AUC, confusion matrix analysis, and prediction confidence distribution. These metrics were selected to provide both overall and class-wise assessment of classification reliability.

3.4 Segmentation Model: Pseudo-Mask Generation via LayerCAM

Since manually annotated pixel-level masks were not available for the collected C&D waste images, a weakly supervised segmentation strategy was adopted. Pseudo-segmentation masks were generated using LayerCAM, which produces class-discriminative localization maps by combining activation maps with their corresponding gradients. Compared with conventional Grad-CAM, LayerCAM provides finer spatial localization because it performs element-wise multiplication between feature activations and positive gradients before spatial aggregation. This makes it more suitable for identifying irregular waste material regions in field image.

For pseudo-mask generation, the trained DenseNet121–Transformer classification model was used as the localization backbone. The model was wrapped using a gradient-based inference mechanism so that both the final convolutional feature maps and class prediction scores could be extracted simultaneously (X. Chen et al., 2023; Idir et al., 2025). For each image, the gradient of the predicted class score was computed with respect to the final convolutional feature map. The positive gradients were retained using ReLU activation and multiplied with the corresponding feature activations to generate a LayerCAM heatmap. The resulting heatmap was resized to 224×224 pixels, refined using bilateral filtering, and binarized using a threshold value of 0.35. Pixels above the threshold were assigned the predicted material class label, while the remaining pixels were treated as background with class index 5.

The generated pseudo-masks were then used to train a U-Net-based segmentation model. The segmentation architecture followed an encoder–decoder structure, as shown in Figure 2 (Lu et al., 2022). A pre-trained DenseNet121 encoder was used to extract hierarchical image features, while five trainable decoder blocks progressively reconstructed the spatial resolution of the segmentation mask. Skip connections from the encoder were concatenated with corresponding decoder layers to preserve fine spatial details and improve boundary reconstruction.

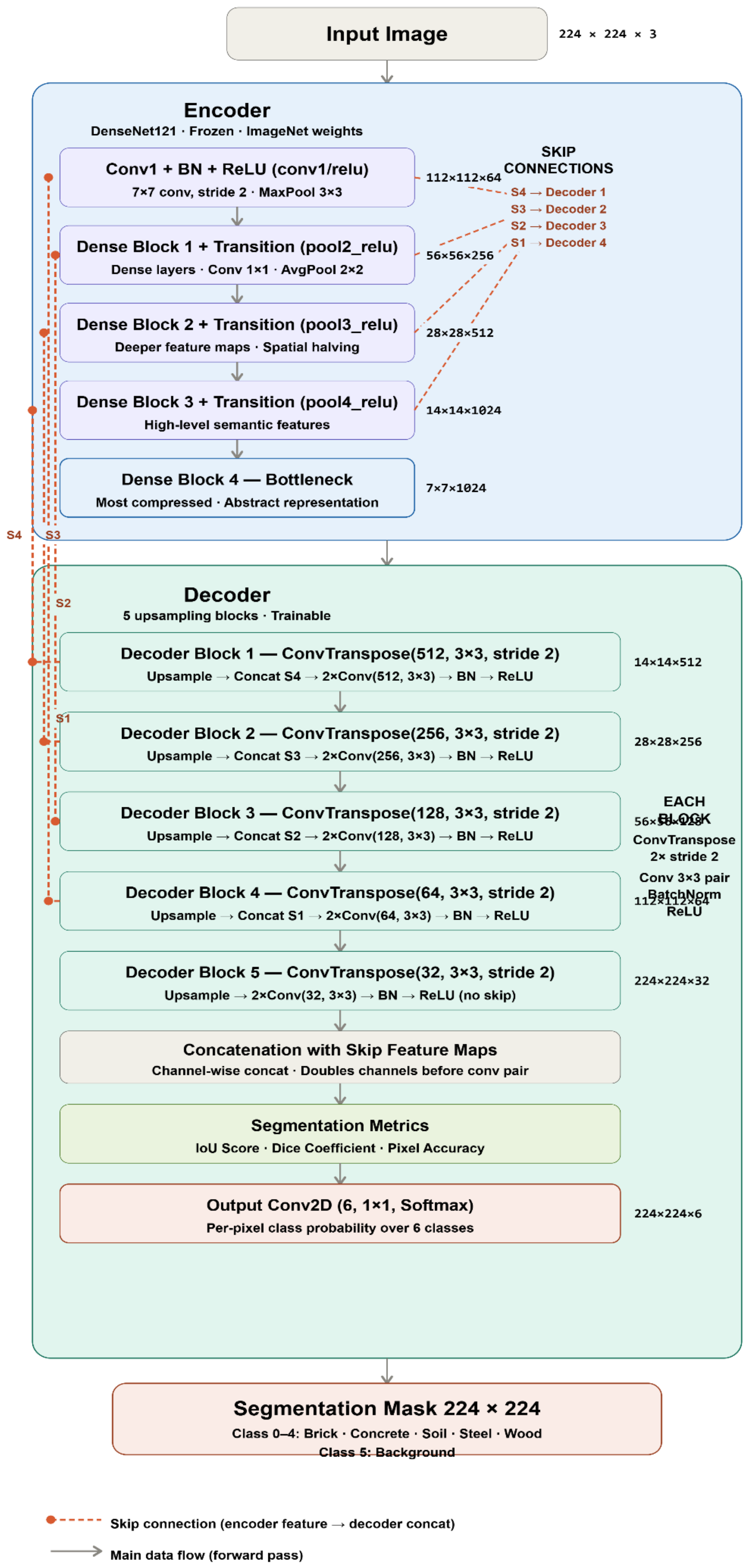

Figure 2. Segmentation Model Architecture:

Table 6. U-Net segmentation architecture

Stage	Component	Output Shape	Notes
Encoder	DenseNet121 (frozen)	7×7×1024	ImageNet pre-trained, skip conn. at 4 layers
Skip 1	pool4_relu	14×14×...	Passed to decoder block 1 via concatenation
Skip 2	pool3_relu	28×28×...	Passed to decoder block 2
Skip 3	pool2_relu	56×56×...	Passed to decoder block 3
Skip 4	conv1/relu	112×112×...	Passed to decoder block 4
Decoder 1	ConvTranspose(512)	14×14×512	Upsample 2× + 2×Conv + BN + ReLU
Decoder 2	ConvTranspose(256)	28×28×256	Upsample 2× + 2×Conv + BN + ReLU
Decoder 3	ConvTranspose(128)	56×56×128	Upsample 2× + 2×Conv + BN + ReLU
Decoder 4	ConvTranspose(64)	112×112×64	Upsample 2× + 2×Conv + BN + ReLU
Decoder 5	ConvTranspose(32)	224×224×32	Upsample 2× + 2×Conv + BN + ReLU
Output	Conv2D(6, 1×1, softmax)	224×224×6	6 classes: 5 materials + background

Table 7. Segmentation Model Training Parameters

Parameter	Value
Loss	Sparse Categorical Cross-Entropy
Optimiser	Adam, LR = 1×10^{-4}
Batch size	16

Max epochs	30 (EarlyStopping patience=10)
LR schedule	ReduceLROnPlateau (factor 0.5, patience=5)
Checkpoint monitor	val_iou_score (maximise)
Encoder weights	Frozen during segmentation training
Augmentation	Flip, rotation (±15°), brightness (±15%), zoom (10%)

The DenseNet121 encoder was kept frozen during segmentation training to retain the general visual features learned from ImageNet, while only the decoder blocks were trained to reconstruct material boundaries from the LayerCAM-generated pseudo-masks. Sparse categorical cross-entropy was used as the loss function because the segmentation task involved pixel-wise multi-class classification across six labels (Aftab et al., 2024; L. Akanbi et al., 2020). Joint image-mask augmentation was applied during training so that transformations such as flipping, rotation, brightness variation, and zoom were applied consistently to both the image and its corresponding pseudo-mask.

Segmentation performance was evaluated using mean Intersection-over-Union (IoU), Dice coefficient, pixel accuracy, and per-class IoU (Ajayi et al., 2015; Shahid & Ali, 2025). These metrics were selected because accuracy alone can be misleading in segmentation tasks where background pixels dominate. Mean IoU and Dice coefficient provide a more reliable assessment of material-region overlap and boundary quality.

3.5 Depth Estimation and Volume Reconstruction: Monocular Depth Estimation

Depth estimation was performed from a single RGB image using a monocular depth estimation approach. Depending on hardware availability, the system used either the MiDaS v2.1 Small model as the primary method or a gradient-based fallback method when GPU-supported inference was unavailable (Zimmermann et al., 2021). This dual-mode strategy ensured that the proposed framework could operate both in GPU-enabled environments and in limited-resource settings.

In the primary mode, the MiDaS v2.1 Small model was loaded through PyTorch Hub for monocular depth prediction. The model generated an inverse depth map from the input RGB image, which was then resized to 224 × 224 pixels using bilinear interpolation and normalized to the range [0, 1]. MiDaS was preferred when CUDA-enabled GPU support was available because it provides more robust relative depth estimation than traditional image-processing-based approximations.

When MiDaS was unavailable, a gradient-based fallback method was used. In this approach, the RGB image was converted to grayscale, and Sobel filters were applied in the horizontal and vertical directions to estimate edge magnitude. A Gaussian smoothing filter with a 21 × 21 kernel was then used to diffuse local gradient information across the image (Paz & Lafayette, 2016; Qiao et al., 2024). The resulting gradient map was inverted to obtain an approximate relative depth representation. Although this fallback does not provide true geometric depth, it enables basic spatial estimation when deep learning-based depth inference cannot be executed.

To reduce boundary noise in the raw depth output, the predicted depth map was refined using the segmentation mask generated in the previous stage. First, a bilateral filter with d = 9, σcolour = 75, and σspace = 75 was applied to smooth the depth map while preserving edges. For each detected material region, the median depth value within the corresponding mask was computed. The final refined depth value was obtained by blending 70% of the original pixel-level depth with 30% of the regional median depth, thereby reducing local outliers while maintaining spatial variation. Background pixels, represented by class index 5, were excluded from the material-specific depth refinement and volume calculation (Hasibuan et al., 2025; Song et al., 2017).

A pinhole-camera-based spatial calibration approach was then used to convert pixel-level measurements into metric units. The calibration parameters used for volume reconstruction are summarized in Table 8.

Table 8. Spatial calibration parameters for volume reconstruction

Parameter	Value	Derivation
Camera height (H)	3.0 m	Fixed field protocol
Horizontal FOV (θ)	60°	Device specification
Ground width at H	2H·tan(θ/2) m	Trigonometric projection
Metres per pixel	Ground width / 224 m/px	≈0.03082 m/px at H=3m, FOV=60°
Area per pixel	(m/px)² m²	≈0.000950 m²/px
Depth scale factor	1.5 m	Max scene depth normalisation constant

For each material class **k**, the volume was estimated by combining the number of segmented pixels, calibrated pixel area, and mean refined depth value. The volume was computed as:

$$V_k = N_k \times A_{pixel} \times \left(\bar{d}_k \times D_{scale}\right)$$

where $V_k$represents the estimated volume of material class k, $N_k$is the number of pixels assigned to that material class, $A_{pixel}$is the calibrated area represented by each pixel in square metres, $\bar{d}_k$is the mean normalized depth value for the material region, and $D_{scale}$is the depth scale factor used to convert normalized depth into approximate metric depth.

This procedure enabled material-wise three-dimensional volume reconstruction from a single field image by integrating segmentation-based spatial localization with monocular depth estimation (Cha et al., 2020; Martins et al., 2026). However, the estimated volumes should be interpreted as calibrated approximations rather than survey-grade measurements, because monocular depth estimation provides relative depth unless externally validated with ground-truth measurements.

3.6 CO_2 Emission Estimation

The material-wise CO_2 emissions were estimated using the reconstructed volume obtained from the segmentation and depth-estimation pipeline. A volume-based emission factor approach was adopted, where each detected material was assigned a specific CO_2 emission factor expressed in kg CO_2 per m^3 (Gao et al., 2024). This approach reduces the additional uncertainty that may arise when converting estimated volumes into mass before emission calculation. However, material density values were also retained to support parallel waste-mass estimation for disposal, recycling, and resource-recovery planning.

The emission factors and density values used in the proposed system are presented in Table 9 (B. Huang et al., 2018; L. Huang et al., 2020). Among the considered C&D waste materials, steel has the highest emission intensity because of its energy-intensive production process, whereas wood is treated as carbon-negative due to its carbon-sequestration potential during growth.

Table 9. Material properties and CO_2 emission factors

Material	Density (kg/m³)	CO_2 Factor (kg/m³)	CO_2 Factor (kg/kg)	Carbon Status
Brick	1,800	+240.0	+0.22	Positive
Concrete	2,400	+300.0	+0.11	Positive
Soil	1,600	+50.0	+0.03	Positive (low)
Steel	7,850	+15700	+2.00	Highly Positive
Wood	600	−360.0	−0.60	Carbon Negative

For each material class k, the CO_2 emission was calculated by multiplying the estimated material volume by the corresponding volume-based emission factor:

$$CO_{2k} = V_k \times EF_k$$

where CO_{2k} denotes the CO_2 emission for material class k in kilograms, V_k represents the estimated material volume in cubic metres, and EF_k is the material-specific emission factor in kg CO_2/m³.

The total net CO_2 emission for an image was computed as the algebraic sum of emissions across all detected material classes:

$$CO_{2,total} = \sum_{k=1}^{n} CO_{2k}$$

This formulation allows carbon-negative materials such as wood to partially offset emissions generated by high-carbon materials such as steel, concrete, and brick. In addition to CO_2 estimation, the system also calculated material mass for waste-management planning using the following equation:

$$M_k = V_k \times \rho_k$$

where M_k is the estimated mass of material class k, V_k is the reconstructed volume, and ρ_k is the material density in kg/m³.

The estimated CO_2 emissions were further converted into practical environmental equivalences, including car-kilometre equivalent, number of trees required for one-year offset, annual household energy equivalent, and short-haul flight equivalent. These indicators improve interpretability for smart-city officers, policymakers, and field engineers by translating technical emission values into more understandable sustainability metrics (Davis et al., 2021; Liu et al., 2019).

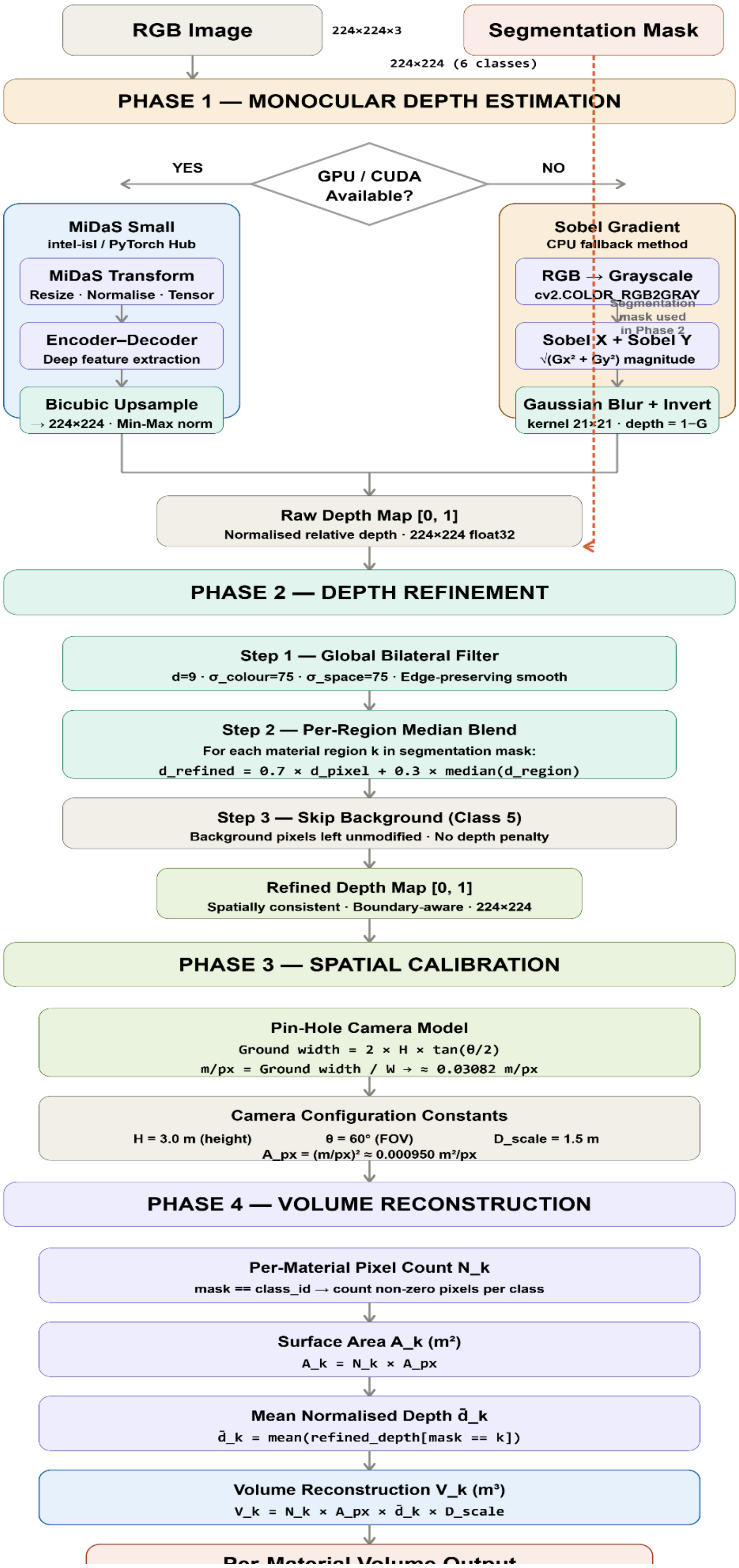

Figure 3. Depth Model Architecture

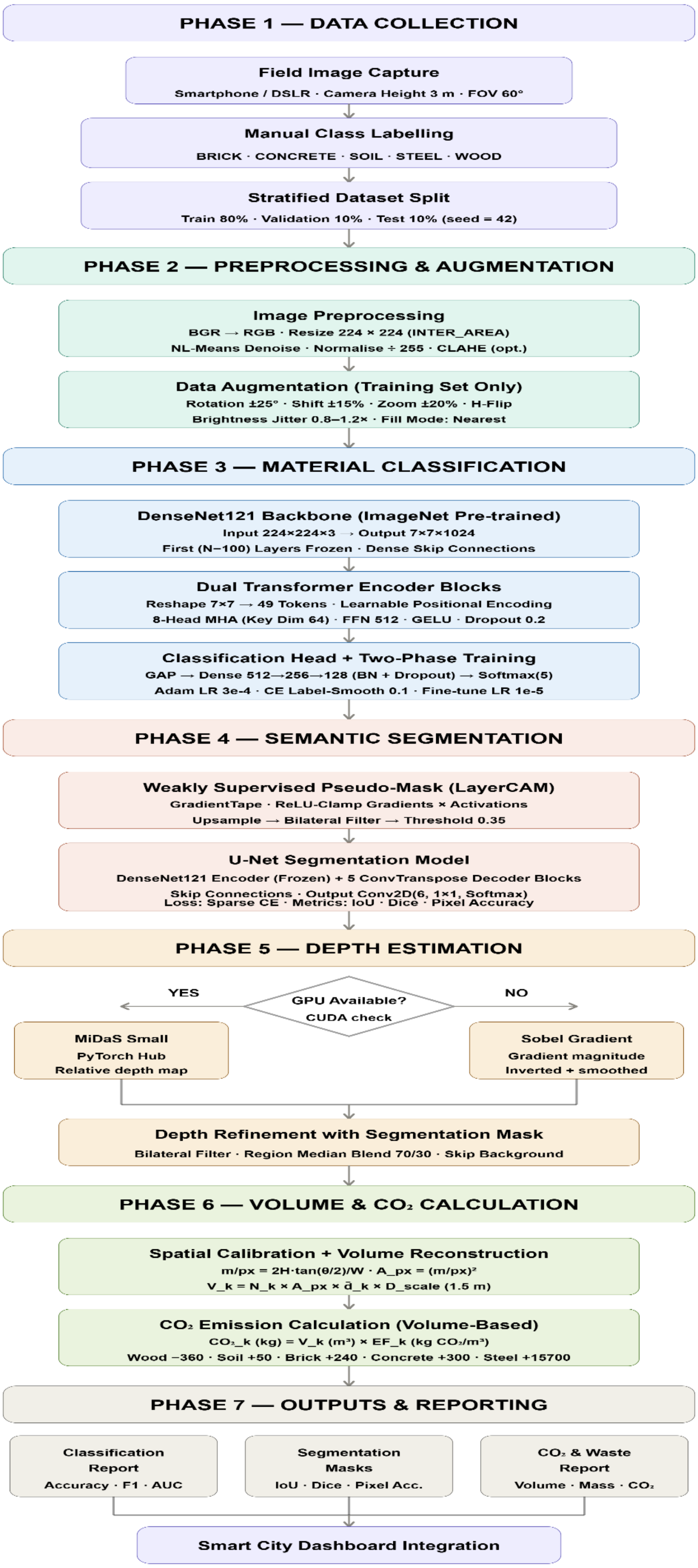

Figure 4. Full Flowchart

4. Results and Discussion

4.1 Dataset Visualization and Image Preprocessing

Figure 5 presents representative sample images from the five C&D waste material categories, namely brick, concrete, soil, steel, and wood. The samples show considerable variation in texture, colour, pile shape, illumination, background conditions, and camera viewpoint. Brick images generally contain reddish fragmented masonry units, concrete images include grey rubble and broken slabs, soil images show granular earth material, steel images contain metallic scrap and reinforcement-like waste, and wood images include timber fragments and discarded wooden pieces (Cha et al., 2021; Sosunova & Porras, 2022). This visual diversity reflects realistic field conditions and justifies the use of deep learning-based feature extraction for material recognition.

The preprocessing outputs are shown in Figure 6. The raw images were resized to a uniform resolution of 224 × 224 pixels, converted into RGB format, denoised, and normalized before being supplied to the neural network. The preprocessing step improved input consistency while retaining important surface-level texture features such as roughness, edges, colour gradients, and material-specific patterns. These features are especially important because several C&D materials, such as concrete, brick, and soil, can appear visually similar under field conditions.

To improve model generalization, data augmentation was applied to the training images, as illustrated in Figure 7 (Araiza-Aguilar et al., 2021; Dong et al., 2022). The augmentation process generated modified versions of the original images using rotation, shifting, zooming, horizontal flipping, and brightness variation. These transformations simulate common field-image variations caused by different camera angles, distances, lighting conditions, and object positions. As a result, the augmented dataset helped reduce overfitting and improved the model's ability to recognize C&D waste materials under practical site conditions.

Figure 5. Sample Images

Figure 6. Pre-processed Images

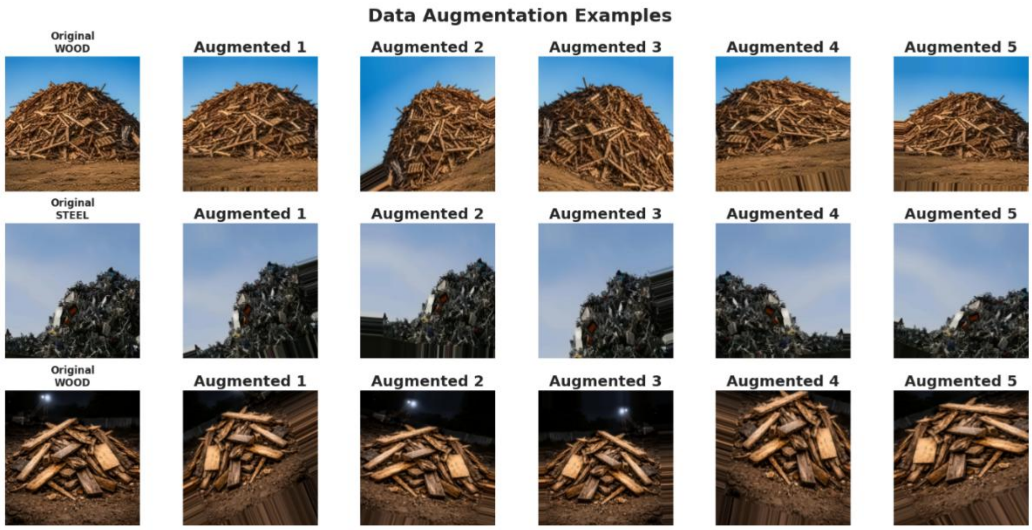

Figure 7. Augmented Images

4.2 Material Classification Model Results

The DenseNet121–Transformer classification model was evaluated on the independent test set containing 102 images. Although the model was configured for a maximum of 30 epochs in the initial training phase and 30 epochs in the fine-tuning phase, training stopped earlier due to callback-based convergence control (Cha et al., 2020; B. Huang et al., 2018). The final training accuracy was 0.9134, while the validation accuracy reached 0.8713, with a validation loss of 0.7148. The overfitting gap was limited to 0.0421, indicating that the model maintained reasonable generalization on unseen validation data.

As shown in Figure 8, the training and validation loss decreased sharply during the initial epochs and then stabilized after fine-tuning. The validation accuracy remained close to the training accuracy, suggesting that the use of transfer learning, dropout, batch normalization, label smoothing, and data augmentation helped control overfitting (Martins et al., 2026; Sosunova & Porras, 2022).

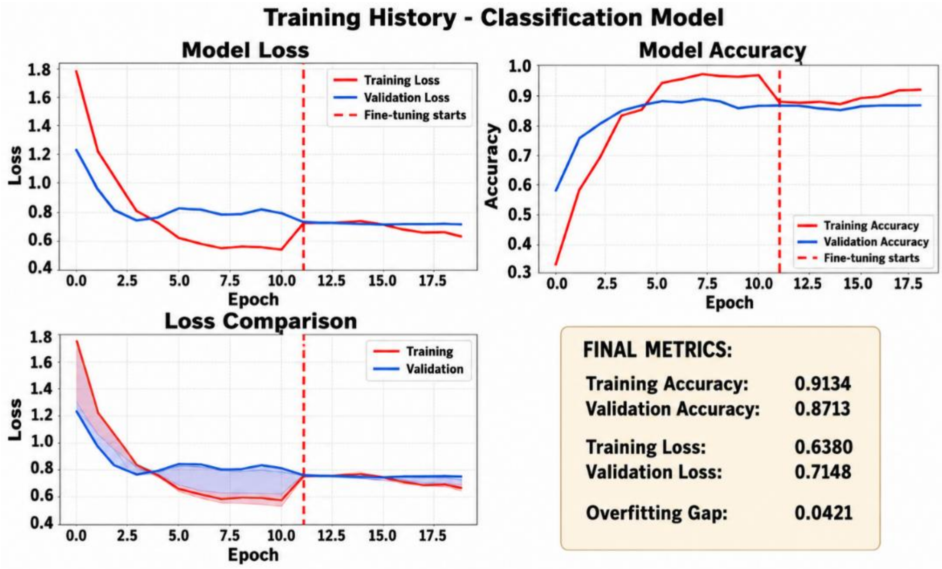

Figure 8. Training Plots

The final test results are presented in Table 10. The model achieved an overall test accuracy of 87.25%, with a weighted F1-score of 0.8730. Among the five material categories, the best classification performance was obtained for steel and soil, with F1-scores of 0.9231 and 0.9167, respectively (L. Huang et al., 2020). Wood also showed strong classification performance with an F1-score of 0.9000. Concrete obtained the lowest F1-score of 0.7907, mainly due to visual similarity with brick and soil waste in mixed field conditions.

Table 10. FINAL TEST RESULTS

Category	Support	Precision	Recall	F1-Score	Specificity	TP	FP	FN	TN
Brick	17	0.8235	0.8235	0.8235	0.9647	14	3	3	82
Concrete	21	0.7727	0.8095	0.7907	0.9383	17	5	4	76
Soil	23	0.8800	0.9565	0.9167	0.9620	22	3	1	76
Steel	20	0.9474	0.9000	0.9231	0.9878	18	1	2	81
Wood	21	0.9474	0.8571	0.9000	0.9877	18	1	3	80

The summary classification metrics are shown in Table 11. The macro-average F1-score of 0.8708 and weighted-average F1-score of 0.8730 were close to the overall accuracy, confirming that the model performed consistently across classes despite minor differences in class support. The micro-average precision, recall, and F1-score were all 0.8725, which is identical to the overall accuracy because each test image was assigned to a single class.

Table 11. Classification Report

Class	Precision	Recall	F1-Score	Support
Brick	0.8235	0.8235	0.8235	17
Concrete	0.7727	0.8095	0.7907	21
Soil	0.8800	0.9565	0.9167	23
Steel	0.9474	0.9000	0.9231	20
Wood	0.9474	0.8571	0.9000	21
Accuracy	—	—	0.8725	102
Macro Average	0.8742	0.8693	0.8708	102
Weighted Average	0.8756	0.8725	0.8730	102

The one-versus-rest AUC values further confirmed the discriminative ability of the classifier. Wood achieved the highest AUC of 0.9918, followed by steel (0.9890), soil (0.9785), concrete (0.9782), and brick (0.8900). The micro-average AUC was 0.9674, indicating strong overall separability among the five material classes.

The confusion matrix in Figure 9 shows that most classes were correctly classified, with limited misclassification across visually similar materials (Araiza-Aguilar et al., 2021; Sosunova & Porras, 2022). The main errors occurred between concrete and brick, brick and soil, and wood and concrete. These errors are expected in field images because broken concrete, dusty brick fragments, and mixed debris piles often share similar colour and texture features.

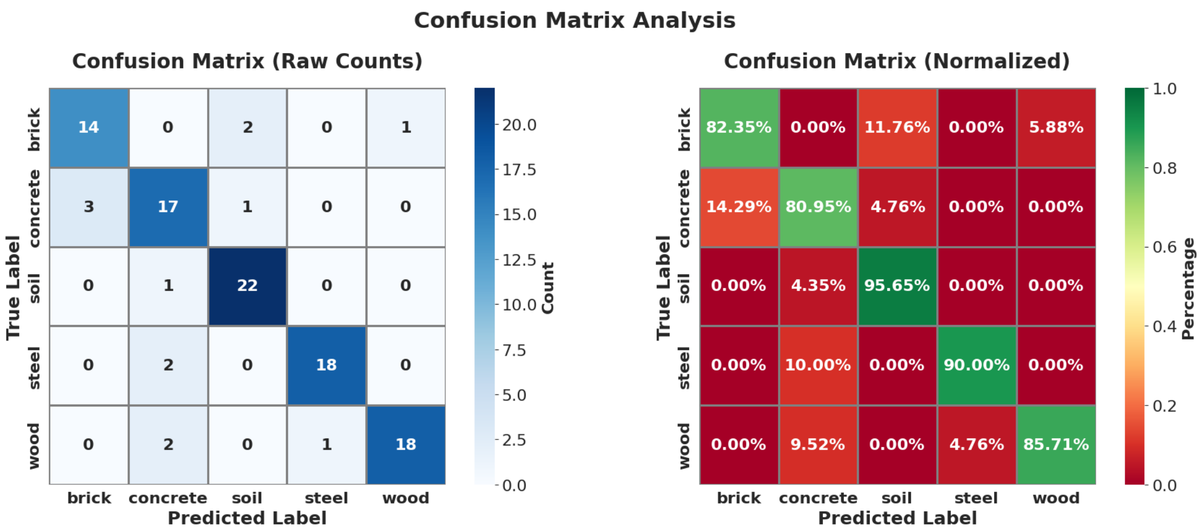

Figure 9. Confusion Matrix

Prediction confidence analysis showed that correct predictions had a mean confidence of 0.8489, whereas incorrect predictions had a lower mean confidence of 0.5841. This gap indicates that the model was generally more certain when making correct classifications and less confident when handling ambiguous or visually mixed waste images (Martins et al., 2026; Paz & Lafayette, 2016). These findings support the reliability of the proposed classification model for automated C&D waste material recognition under practical field conditions.

4.3 ROC Analysis, Confidence Assessment and Error Analysis

The discriminative capability of the DenseNet121–Transformer classifier was further evaluated using one-versus-rest ROC analysis, as shown in Figure 10. The model achieved a strong micro-average AUC of 0.967, indicating high overall class separability across the five C&D waste categories (Dong et al., 2022; Lu & Tam, 2013). Among the individual classes, wood obtained the highest AUC value of 0.992, followed by steel at 0.989, soil at 0.979, and concrete at 0.978. Brick showed the lowest AUC value of 0.890, suggesting that brick was relatively more difficult to distinguish from visually similar debris classes such as concrete and soil.

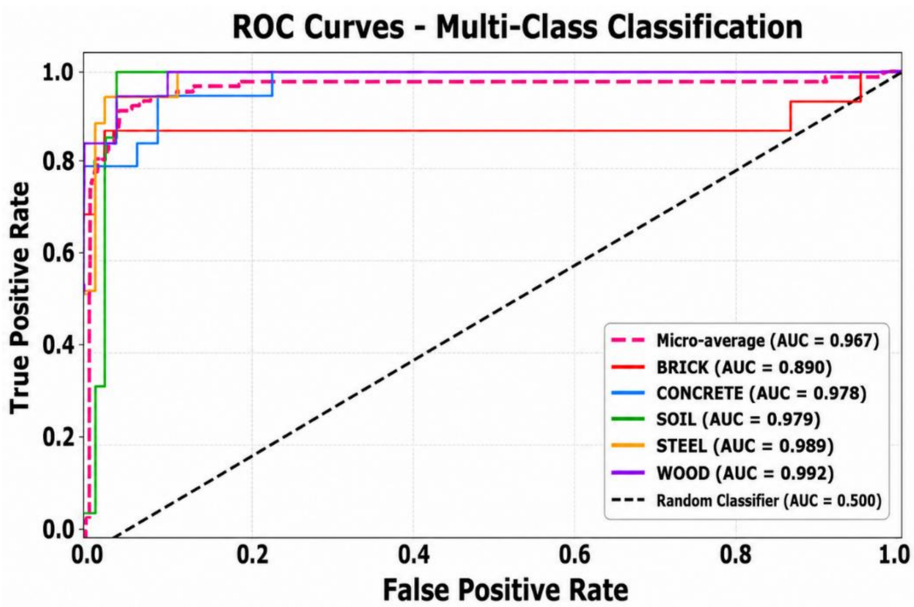

Figure 10. ROC Curve

The correct prediction examples shown in Figure 11 demonstrate that the model successfully identified material categories when visual features were clear and class-specific (Cha et al., 2022; J. Li et al., 2022). High-confidence correct predictions were observed for soil, wood, concrete, and brick samples, indicating that the classifier effectively learned major textural and colour-based patterns. However, some correct predictions were made with moderate confidence, especially for visually mixed or partially occluded waste piles, showing that field conditions still introduce ambiguity.

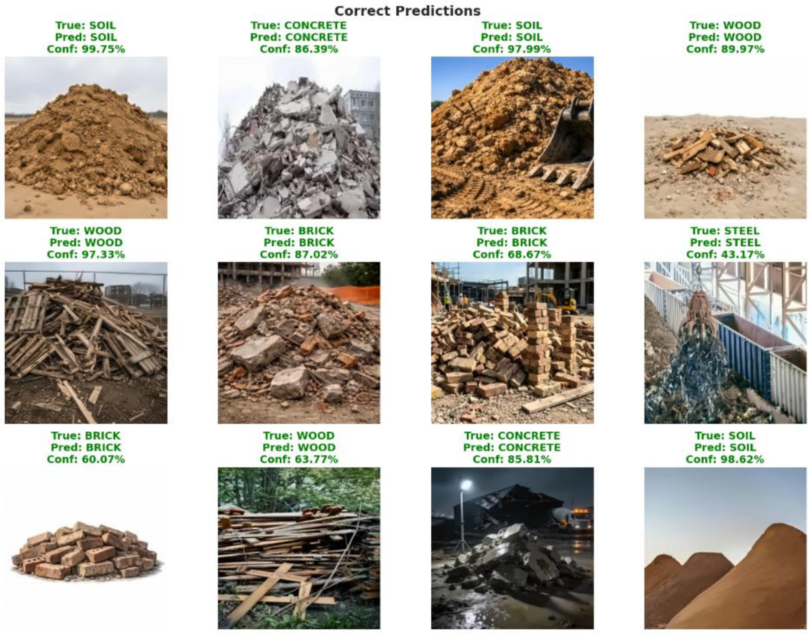

Figure 11. Correct Prediction

The incorrect prediction examples in Figure 12 reveal that most errors occurred in images containing mixed waste, poor lighting, overlapping materials, or visually similar textures. Concrete was sometimes misclassified as brick or soil because broken concrete rubble and brick fragments often share similar grey–brown colour tones and irregular surface structures. Similarly, steel was occasionally predicted as concrete when metallic scrap appeared mixed with dust, debris, or construction residue (Lakhouit, 2025).

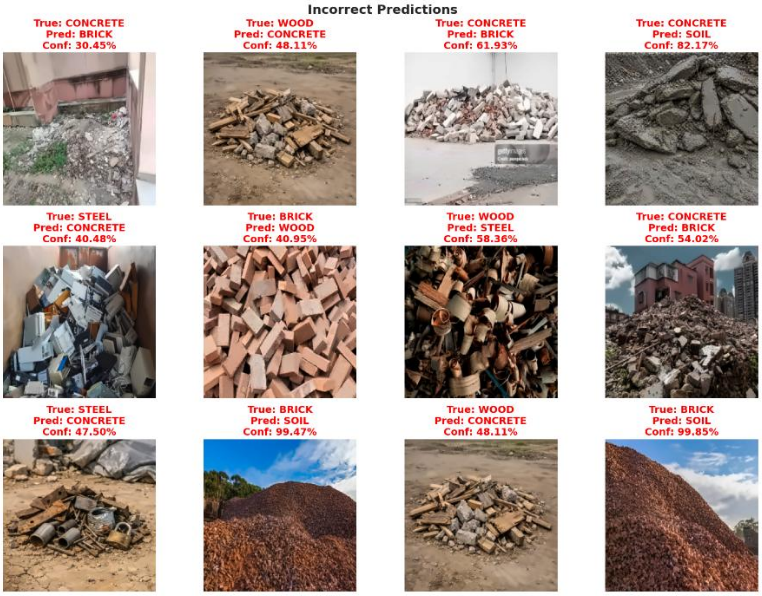

Figure 12. Incorrect Prediction

Figure 13 presents low-confidence predictions below 60%. These examples are important because they identify cases where the model was uncertain rather than confidently wrong. Low-confidence predictions were mainly associated with mixed material piles, cluttered backgrounds, and ambiguous visual patterns. This suggests that confidence scores can be useful in a practical deployment setting: images with low confidence can be flagged for manual verification by field officers rather than being accepted automatically.

Figure 13. Low Confidence Prediction

The most frequent misclassification patterns are summarized in Table 12. The highest misclassification occurred for concrete predicted as brick, with three cases, representing 14.29% of concrete samples. Brick was also misclassified as soil in two cases, while wood and steel were occasionally confused with concrete. These errors are understandable but not ignorable; they show that the model performs well overall, but still struggles when material boundaries are unclear or when debris piles contain mixed visual characteristics.

Table 12. Most Common Misclassifications

True Class	Predicted As	Count	Percentage (%)
Concrete	Brick	3	14.29
Brick	Soil	2	11.76
Wood	Concrete	2	9.52
Steel	Concrete	2	10.00
Concrete	Soil	1	4.76
Brick	Wood	1	5.88
Soil	Concrete	1	4.35
Wood	Steel	1	4.76

Overall, the ROC and confidence analyses confirm that the proposed classifier achieved strong material discrimination, but the error analysis also exposes the main weakness of the model: confusion among visually similar or mixed C&D materials. Therefore, while the model is suitable for automated field-level screening, low-confidence predictions should be treated as review cases in real deployment rather than final outputs.

4.4 Weakly Supervised Segmentation Performance

The segmentation model was trained using LayerCAM-generated pseudo-masks because manually annotated pixel-level ground-truth masks were not available. The generated pseudo-masks were used as weak supervision for training the DenseNet121-based U-Net segmentation model (Lee et al., 2016; Lu & Tam, 2013). The class-wise pixel distribution of the training and validation pseudo-masks is presented in Tables 13 and 14, respectively. In both subsets, background pixels accounted for nearly half of the total pixels, indicating that the pseudo-mask generation process separated material regions from non-material regions with a reasonably balanced foreground–background distribution.

Table 13. Training Mask Class Distribution

Class	Pixel Count	Percentage (%)
Brick	1,014,398	10.01
Concrete	1,114,849	11.00
Soil	970,144	9.57
Steel	1,233,794	12.17
Wood	692,272	6.83
Background	5,110,095	50.42
Total	10,135,552	100.00

Table 14. Validation Mask Class Distribution:

Class	Pixel Count	Percentage (%)
Brick	1,053,052	10.39
Concrete	1,049,739	10.36
Soil	824,637	8.14
Steel	1,195,543	11.80
Wood	867,006	8.55
Background	5,145,575	50.77
Total	10,135,552	100.00

The mask coverage statistics are summarized in Table 15. The mean material coverage was 49.58% for the training set and 49.23% for the validation set, showing that the generated pseudo-masks maintained comparable foreground representation in both subsets (X. Chen et al., 2023; Lakhouit, 2025). However, the high standard deviation values indicate considerable variation in visible waste-material coverage across images, which is expected in uncontrolled field conditions where waste piles differ in size, distance, and background clutter.

Table 15. Mask Coverage Statistics

Statistic	Training Set	Validation Set
Mean Coverage (%)	49.58	49.23
Median Coverage (%)	50.43	54.40
Standard Deviation (%)	28.80	26.61
Minimum Coverage (%)	4.04	3.02

Maximum Coverage (%)	99.84	98.15

The segmentation distribution for the independent test set is shown in Table 16. Background pixels formed 71.88% of the test-set pixels, while the remaining pixels were distributed among the five C&D material classes (Ajayi et al., 2015; Lu et al., 2022). Concrete and soil had the highest segmented material shares in the test set, with 10.20% and 10.70%, respectively. Brick, steel, and wood showed comparatively lower pixel representation, which partly explains their weaker class-wise segmentation performance.

Table 16. Test Set Segmentation Distribution:

Class	**Pixel Count**	**Percentage (%)**
Brick	139,828	2.73
Concrete	522,129	10.20
Soil	547,701	10.70
Steel	132,669	2.59
Wood	96,935	1.89
Background	3,678,690	71.88
Total	5,117,952	100.00

The U-Net segmentation model completed 30 training epochs. As shown in Figure 14, the training loss decreased steadily, while validation loss also reduced but remained higher than the training loss. The training IoU and Dice coefficient increased consistently, while the validation curves improved more gradually and then stabilized. The final validation accuracy was 0.6087, the final validation Dice coefficient was 0.6097, and the validation IoU score reached 0.4423. These results indicate that the model learned useful spatial localization patterns from weak pseudo-labels, although the gap between training and validation curves suggests moderate overfitting and the inherent limitation of pseudo-mask supervision (Martins et al., 2026; Song et al., 2017).

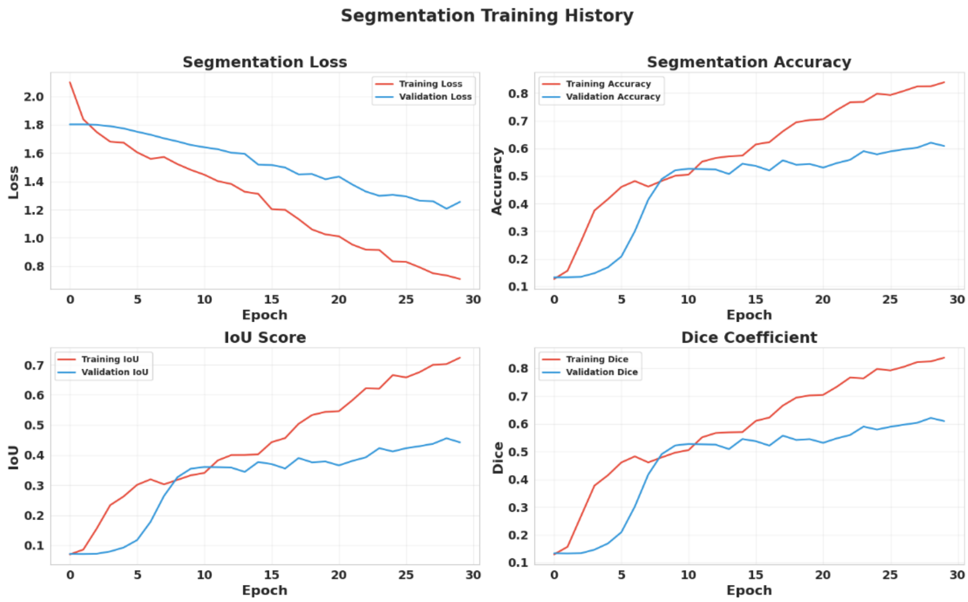

Figure 14. Segmentation Training History Curve

The per-class IoU results on the validation set are presented in Table 17. Background achieved the highest IoU of 0.5678, followed by soil (0.4216) and concrete (0.3767). Brick obtained a moderate IoU of 0.3082, whereas steel and wood showed lower IoU values of 0.1719 and 0.1915, respectively. The weaker performance for steel and wood is mainly due to their irregular shapes, fragmented boundaries, lower pixel coverage, and frequent overlap with other construction debris. The mean per-class IoU across all six classes was 0.3396.

Table 17. PER-CLASS IoU SCORES (VALIDATION SET)

Class	IoU	Intersection	Union	True Pixels	Predicted Pixels
Brick	0.3082	352,817	1,144,908	1,053,052	444,673
Concrete	0.3767	566,942	1,505,193	1,049,739	1,022,396
Soil	0.4216	625,042	1,482,503	824,637	1,282,908
Steel	0.1719	218,971	1,273,977	1,195,543	297,405
Wood	0.1915	175,071	914,299	867,006	222,364
Background	0.5678	4,350,012	7,661,369	5,145,575	6,865,806

Mean IoU: 0.3396

4.5 Depth Estimation and Three-Dimensional Volume Reconstruction

The depth-estimation output is presented in Figure 15, where each row shows the original image, estimated depth map, segmentation mask, depth overlay, and depth contour for representative C&D waste samples. The results indicate that the monocular depth-estimation module successfully captured the relative spatial structure of waste piles from single RGB images. Elevated material piles generally appear as distinguishable depth regions, while flatter or background regions show lower depth variation (X. Li et al., 2022; Lu & Yuan, 2013). This confirms that the depth-estimation stage provides useful spatial information for subsequent volume reconstruction.

The generated depth maps were normalized within the range [0, 1] before being combined with the segmentation masks. The overall mean depth value was 0.4776, with a standard deviation of 0.2849, indicating moderate variation in estimated depth across the analyzed images. The minimum and maximum normalized depth values were 0.0001 and 0.9985, respectively, showing that the model produced a wide relative depth range suitable for distinguishing foreground material piles from background regions (Paz & Lafayette, 2016; Qiao et al., 2024).

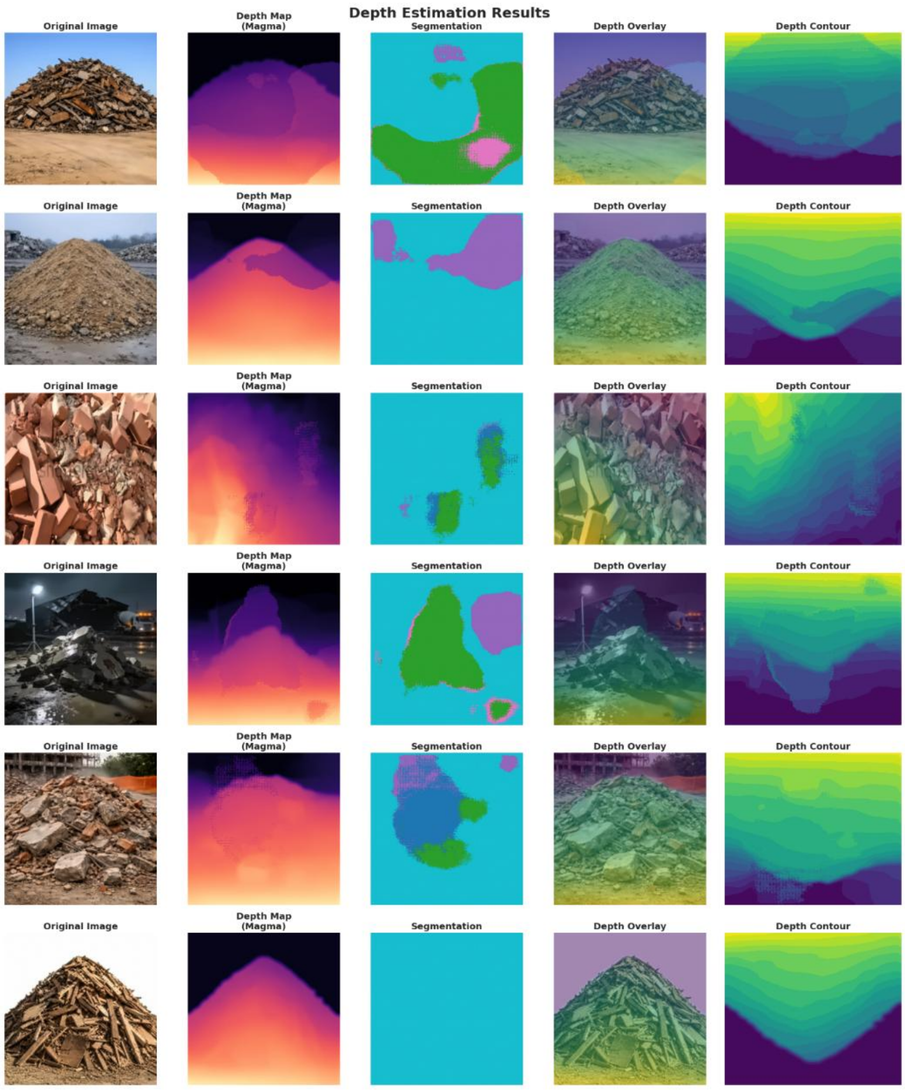

Figure 15. Depth Map

4.6 CO_2 Emission and Sustainability Assessment

The reconstructed material volumes obtained from the segmentation and depth-estimation pipeline were used to estimate material-wise CO_2 emissions for the test dataset. The emission calculation was performed using volume-based CO_2 emission factors, where each material category was assigned a specific emission factor in kg CO_2/m^3 (X. Li et al., 2022; Martins et al., 2026). The adopted emission factors were 240 kg CO_2/m^3 for brick, 300 kg CO_2/m^3 for concrete, 50 kg CO_2/m^3 for soil, 15,700 kg CO_2/m^3 for steel, and −360 kg CO_2/m^3 for wood. Steel was treated as the most carbon-intensive material, while wood was considered carbon-negative because of its carbon-sequestration potential.

As shown in Table 18, the total estimated CO_2 emission for the test dataset was 367,451.61 kg, equivalent to 367.4516 tonnes CO_2. Although steel accounted for only 21.23 m^3 of the total volume, it contributed 333.2328 tonnes CO_2, representing the dominant share of emissions because of its very high emission factor (Davis et al., 2021; B. Huang et al., 2018). In contrast, concrete had the highest volume contribution at 100.97 m^3, but its total CO_2 emission was substantially lower at 30.2898 tonnes. Wood produced a negative CO_2 value of −6.2140 tonnes, partially offsetting the total emissions.

Table 18. Per-Material CO2 Emissions (Test Set):

Material	**Volume (m^3)**	**CO_2 Emissions (kg)**	**CO_2 Emissions (tonnes)**
Brick	27.49	6,596.55	6.5965
Concrete	100.97	30,289.76	30.2898
Soil	70.93	3,546.46	3.5465
Steel	21.23	333,232.84	333.2328
Wood	17.26	−6,213.99	−6.2140
Total	—	367,451.61	367.4516

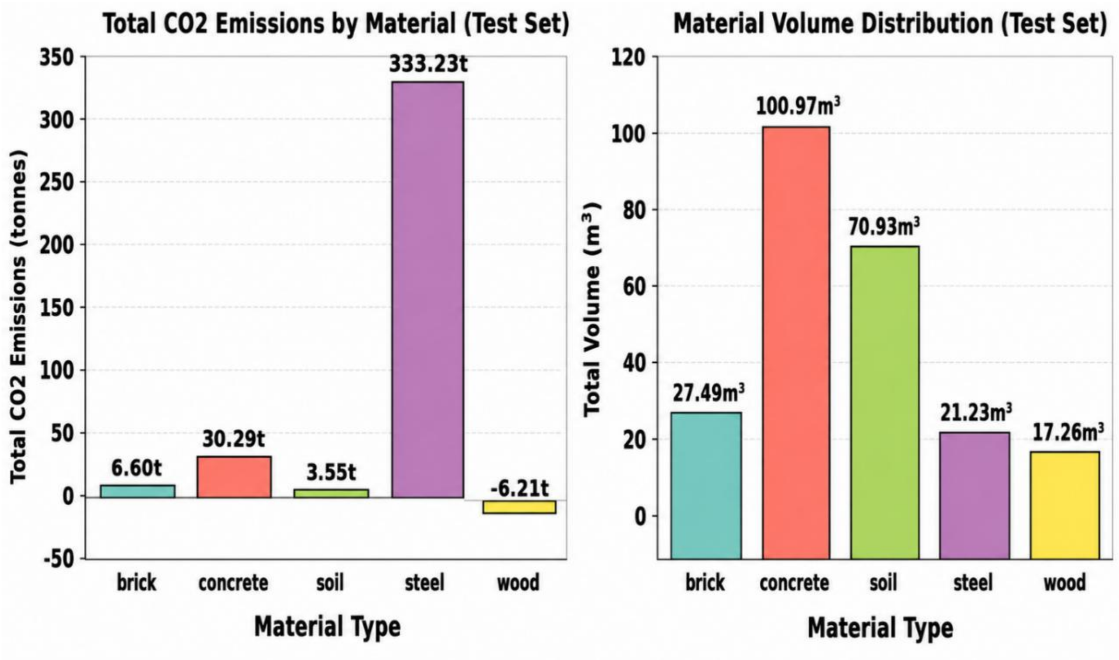

Figure 16. Total CO2 Emission for test Set

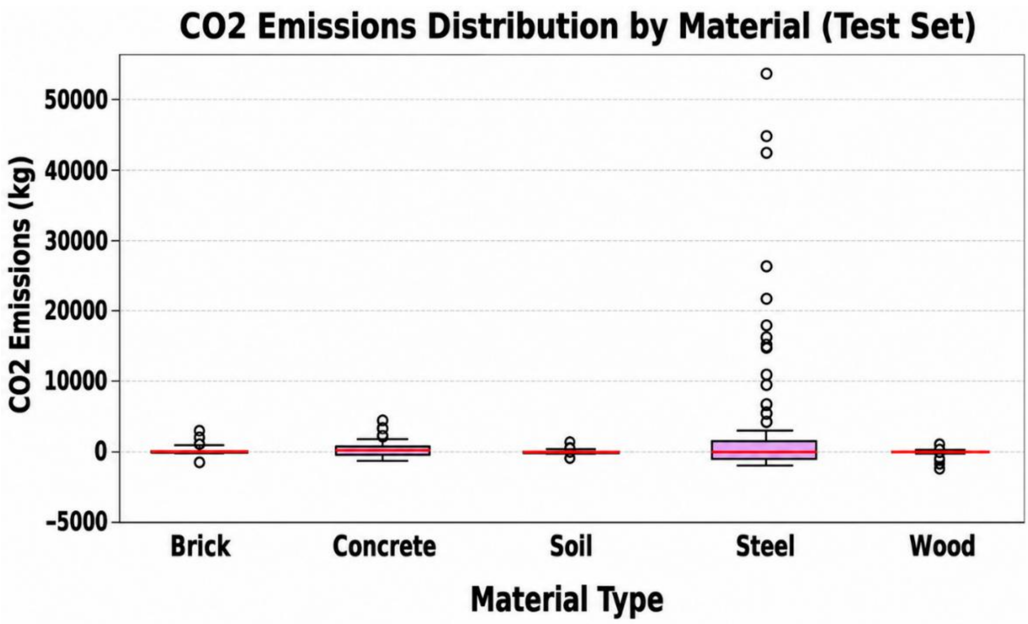

Figure 17. CO2 Emission by material

The material sustainability ranking is presented in Table 19. Wood ranked highest due to its negative CO_2 value, followed by soil because of its low emission intensity (Cha et al., 2021). Brick and concrete were rated as moderate because they contributed positive but relatively lower emissions compared with steel. Steel was ranked lowest because it contributed the highest CO_2 burden despite its lower volume share.

Table 19. Material Sustainability Ranking (Lower CO2 = Better):

Material	Volume (m³)	CO_2 per m³ (kg)	Total CO_2 (kg)	Sustainability Rating
Wood	17.26	−360.0	−6,213.99	Excellent
Soil	70.93	50.0	3,546.46	Good
Brick	27.49	240.0	6,596.55	Moderate
Concrete	100.97	300.0	30,289.76	Moderate
Steel	21.23	15,700.0	333,232.84	Poor

A complete material-wise waste and CO_2 analysis is provided in Table 20. The total estimated waste mass was 582.2519 tonnes, with concrete contributing the largest mass share of 41.62%, followed by steel at 28.62% and soil at 19.49%. However, the CO_2 contribution did not follow the same order as mass (Sosunova & Porras, 2022). Steel alone contributed 90.69% of the total CO_2 emissions, confirming that emission intensity is more important than material quantity when assessing environmental burden.

Table 20. WASTE MATERIAL & CO2 ANALYSIS REPORT

Material	Total Area (m²)	Total Volume (m³)	Total Mass (tons)	Total CO_2 (tonnes)	Mass Share (%)	CO_2 Share (%)	Avg. Classification Confidence	No. of Images
Steel	31.73	21.23	166.62	333.2328	28.62	90.69	0.1485	102
Concrete	124.87	100.97	242.32	30.2898	41.62	8.24	0.2892	61
Brick	33.44	27.49	49.47	6.5965	8.50	1.80	0.2447	53
Wood	23.18	17.26	10.36	−6.2140	1.78	−1.69	0.8592	16
Soil	130.99	70.93	113.49	3.5465	19.49	0.97	0.3732	69

The overall environmental impact of the test set was further converted into practical equivalence indicators. The net emission of 367.4516 tonnes CO_2 is equivalent to approximately 3,062,097 km of car travel, 17,498 trees required for one-year offset, and 81.66 household-energy years. These indicators make the emission output more interpretable for smart-city authorities and field-level decision-makers.

Table 21. DETAILED CO2 EMISSIONS BREAKDOWN

Material	Total CO_2 (kg)	Total CO_2 (tonnes)	CO_2 Factor (kg/m³)	CO_2 Factor (kg/kg)	CO_2 Intensity (kg/m³)	CO_2 Intensity (kg/kg)
Steel	333,232.84	333.2328	15,700.0	2.00	15,700.0	2.0000
Concrete	30,289.76	30.2898	300.0	0.11	300.0	0.1250
Brick	6,596.55	6.5965	240.0	0.22	240.0	0.1333
Wood	−6,213.99	−6.2140	−360.0	−0.60	−360.0	−0.6000
Soil	3,546.46	3.5465	50.0	0.03	50.0	0.0313

Table 22. MATERIAL SUSTAINABILITY RANKING

Material	Total Mass (tons)	Total CO_2 (tonnes)	CO_2 Intensity (kg CO_2/kg Material)	Sustainability Rating
Wood	10.36	−6.2140	−0.6000	Excellent (Carbon Negative)
Soil	113.49	3.5465	0.0313	Good
Concrete	242.32	30.2898	0.1250	Good
Brick	49.47	6.5965	0.1333	Good
Steel	166.62	333.2328	2.0000	Very Poor

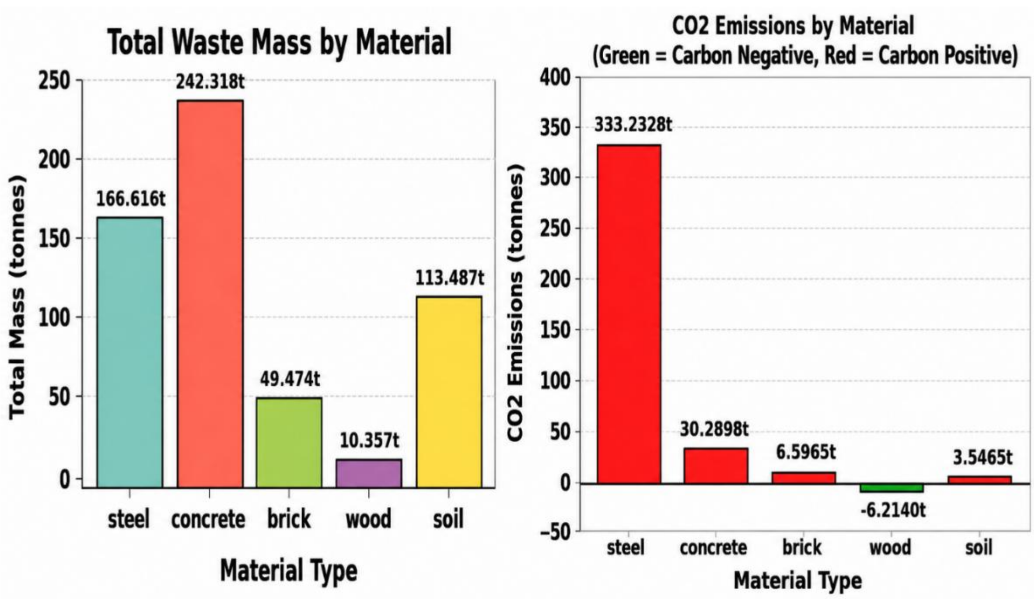

Figure 18. TOTAL WASTE MASS AND CO2 EMISSION BY MATERIAL

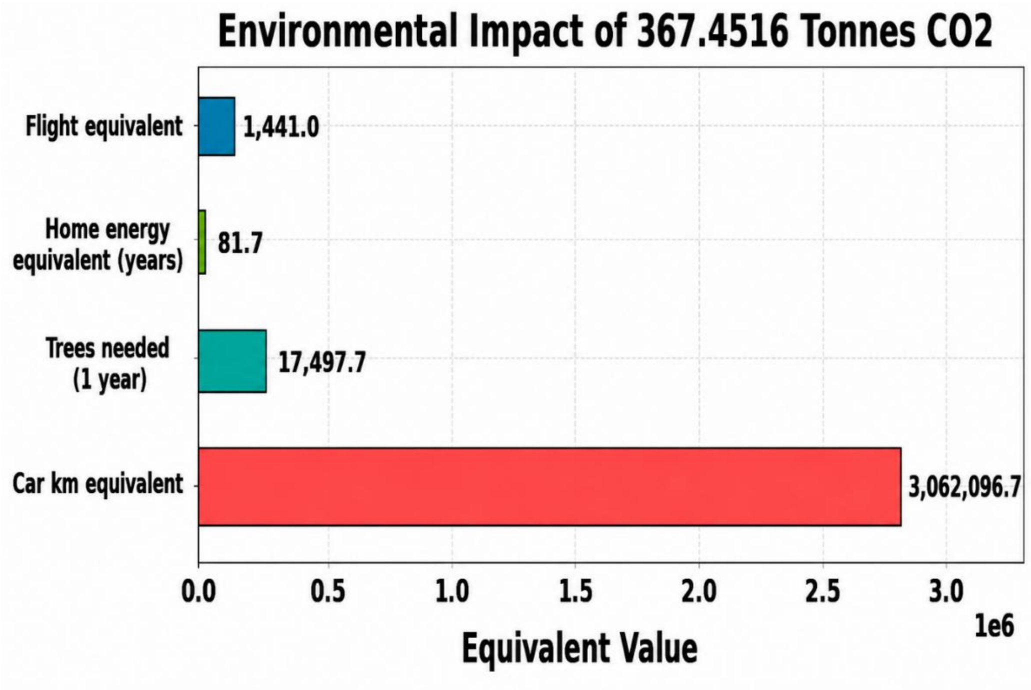

Figure 19. ENVIRONMENTAL IMPACT

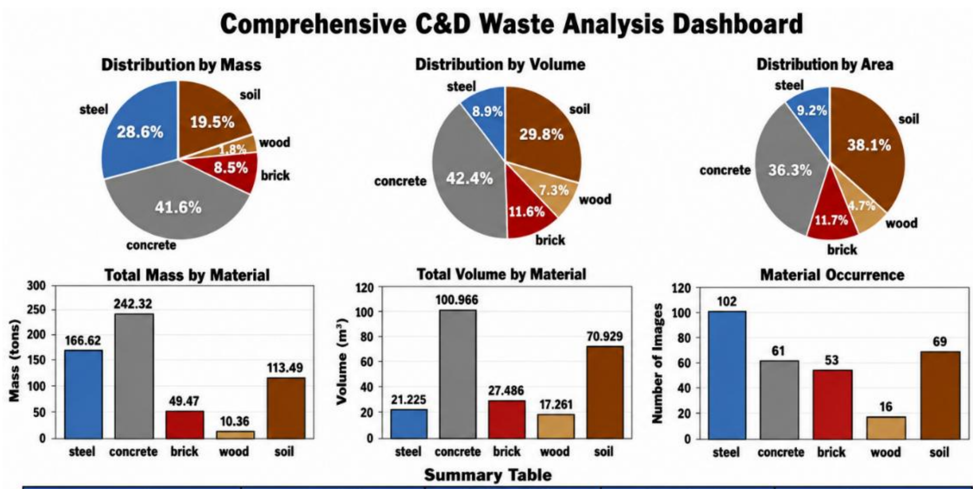

Material	Area (m²)	Volume (m³)	Mass (tons)	% Mass
STEEL	31.73	21.2250	166.62	28.6%
CONCRETE	124.87	100.9659	242.32	41.6%
BRICK	33.44	27.4856	49.47	8.5%
WOOD	23.18	17.2611	10.36	1.8%
SOIL	130.99	70.9291	113.49	19.5%

Figure 20. Dashboard:

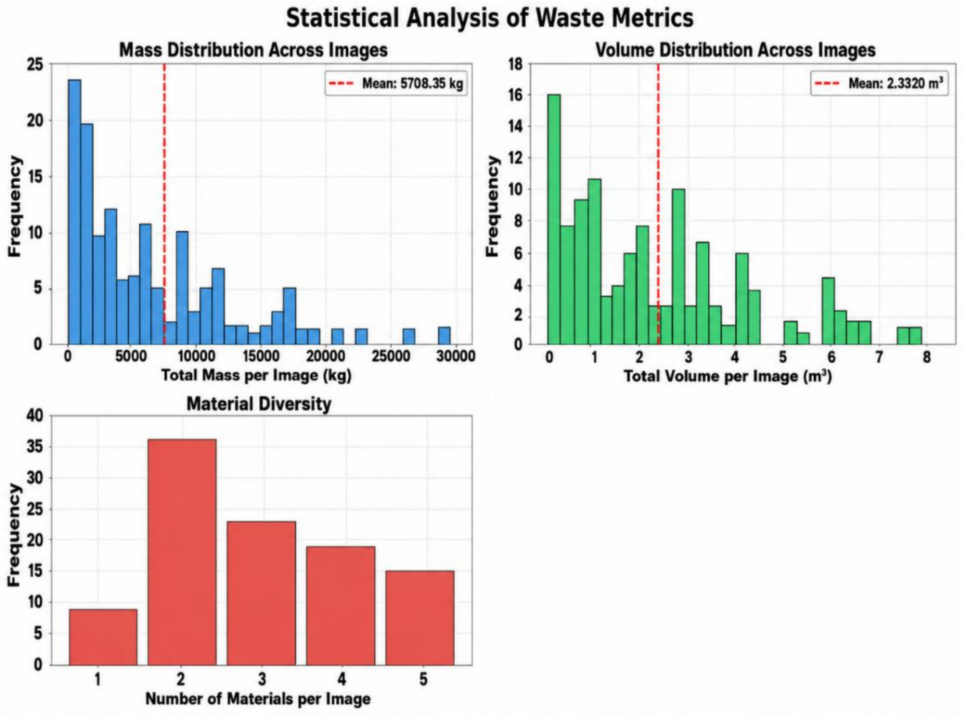

Figure 21. STATISTICAL ANALYSIS:

4.7 Single-Image Demonstration

To demonstrate the practical applicability of the proposed pipeline, a single C&D waste image was processed through the complete inference workflow. The uploaded image, shown in Figure 22, contains a mixed construction debris pile with visible concrete fragments, brick pieces, soil, and scattered steel elements. The model classified the image as concrete with a confidence score of 79.22%, indicating that concrete was the dominant material detected in the scene. The remaining class probabilities were comparatively lower, with brick at 5.45%, soil at 4.09%, steel at 7.47%, and wood at 3.77% (Liu et al., 2019; Lu & Yuan, 2013).

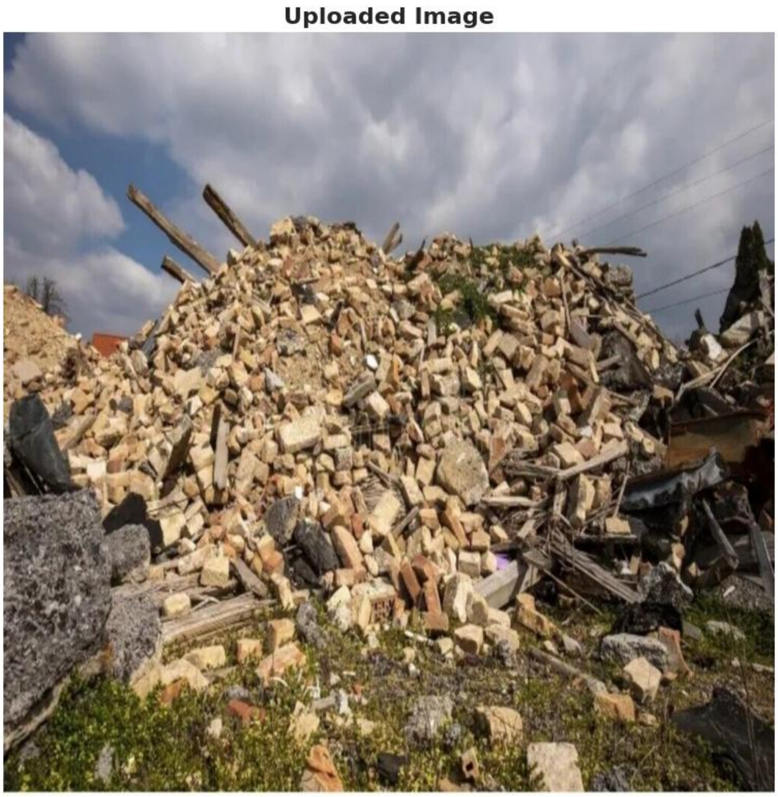

Figure 22. Uploaded Image

The complete waste quantification output is shown in Figure 23. The system generated the segmentation mask, refined depth map, segmentation overlay, material probability chart, material-wise mass distribution, depth contour map, and detailed waste metrics. The analysis confirmed that concrete was the dominant material, contributing 95.3% of the estimated total mass (Martins et al., 2026). The estimated total waste area was 4.2871 m^2, total volume was 2.239709 m^3, total mass was 5,380.137 kg, and total CO_2 emission was 842.023 kg.

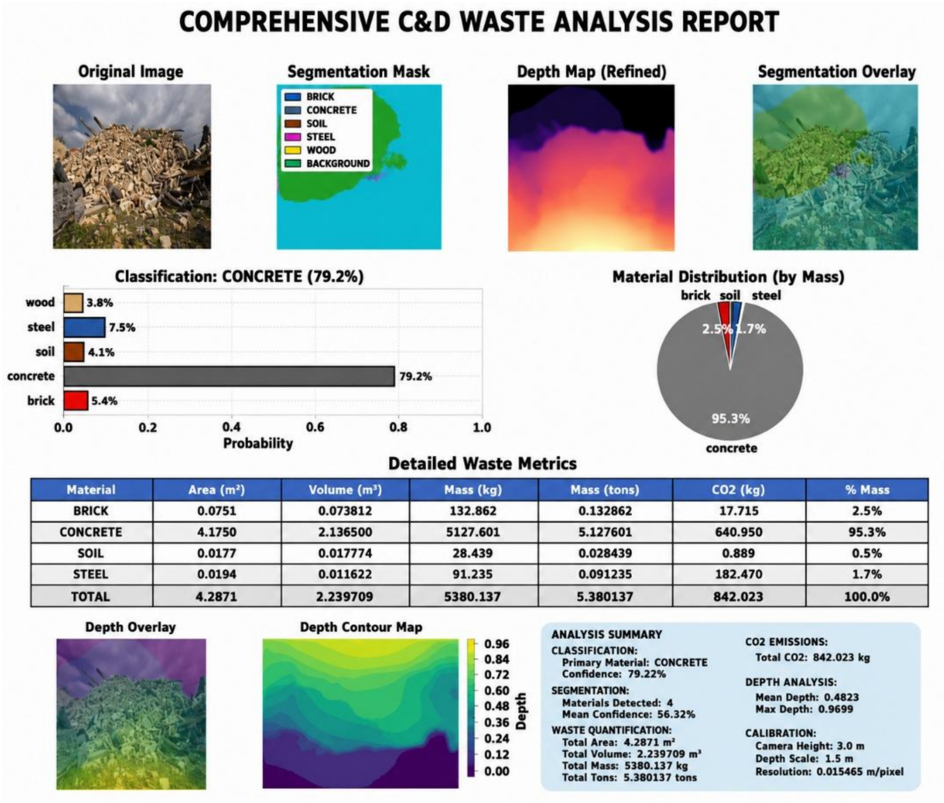

Figure 23. WASTE MATERIAL QUANTIFICATION

Table 23. Material-wise waste quantification for the uploaded image

Material	**Area (m²)**	**Area (%)**	**Avg. Depth (m)**	**Volume (m³)**	**Volume (%)**	**Density (kg/m³)**	**Mass (kg)**	**Mass (tons)**	**Mass (%)**	**CO_2 (kg)**
Brick	0.0751	1.8	0.9829	0.073812	3.3	1,800	132.862	0.132862	2.5	17.715
Concrete	4.1750	97.4	0.5117	2.136500	95.4	2,400	5,127.601	5.127601	95.3	640.950
Soil	0.0177	0.4	1.0043	0.017774	0.8	1,600	28.439	0.028439	0.5	0.889
Steel	0.0194	0.5	0.6000	0.011622	0.5	7,850	91.235	0.091235	1.7	182.470
Total	4.2871	100.0	—	2.239709	100.0	—	5,380.137	5.380137	100.0	842.023

Table 24. Overall summary

Metric	Value
Total Area	4.2871 m^2
Total Volume	2.239709 m^3
Total Mass	5,380.137 kg (5.380137 tons)
Total CO_2 Emissions	842.023 kg (0.842023 tonnes)

4.8 Dashboard Development Model

The proposed Smart City Gwalior C&D Waste Management Dashboard was developed as a role-based digital monitoring platform to support construction and demolition waste reporting, tracking, recycling verification, compliance monitoring, and environmental impact assessment. The dashboard acts as the operational interface of the AI-enabled C&D waste management system by translating technical outputs such as material classification, estimated volume, waste mass, and CO_2 emissions into actionable information for municipal users, waste generators, recyclers, and administrative authorities.

The dashboard begins with a secure sign-in interface, as shown in Figure 24. The login screen allows users to enter their email or user ID, password, and assigned role before accessing the monitoring system. This structure ensures that different user groups interact only with the modules relevant to their responsibilities (Lu & Yuan, 2013; Zimmermann et al., 2021). In the displayed prototype, role options include administrative and municipal-level users such as GMC Administrator, Ward Officer, Review Committee, and Smart City Mission.

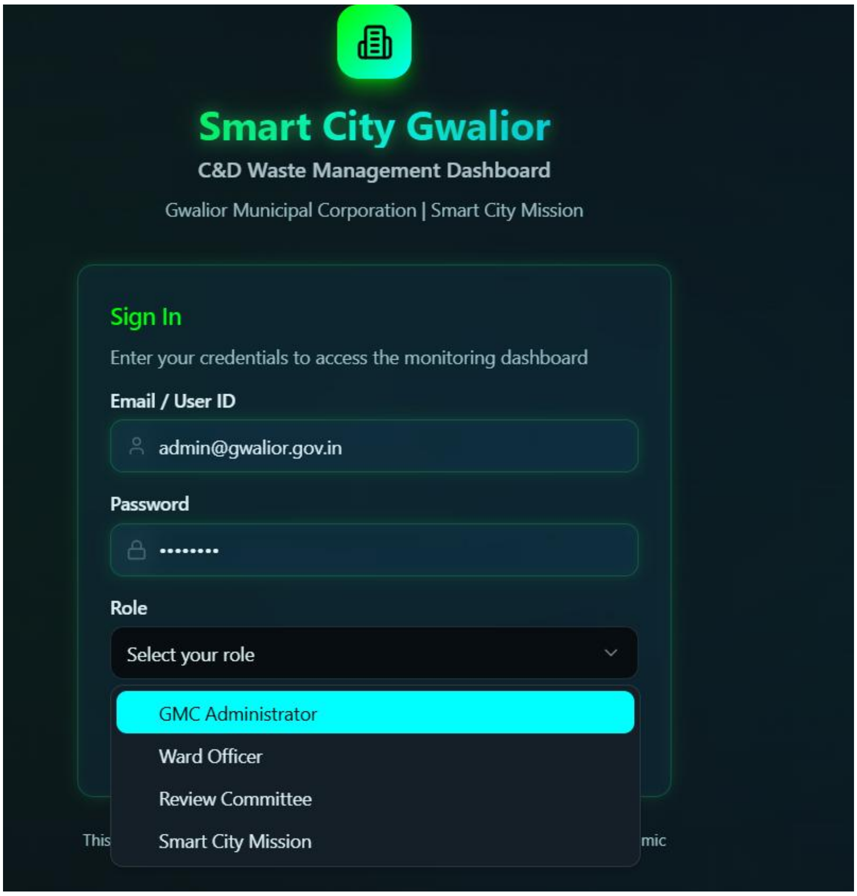

Figure 24. Smart City Gwalior C&D Waste Management Dashboard sign-in interface.

After authentication, the system provides a role-selection interface, as shown in Figure 25. Three functional stakeholder roles are included: Waste Generator, Recycler, and Authority. The Waste Generator role is designed for construction sites, demolition contractors, and agencies that generate C&D waste (Cha et al., 2020). The Recycler role is intended for recycling and waste-processing facilities. The Authority role is designed for municipal officials responsible for reviewing reports, monitoring compliance, and supervising city-level waste management activities.

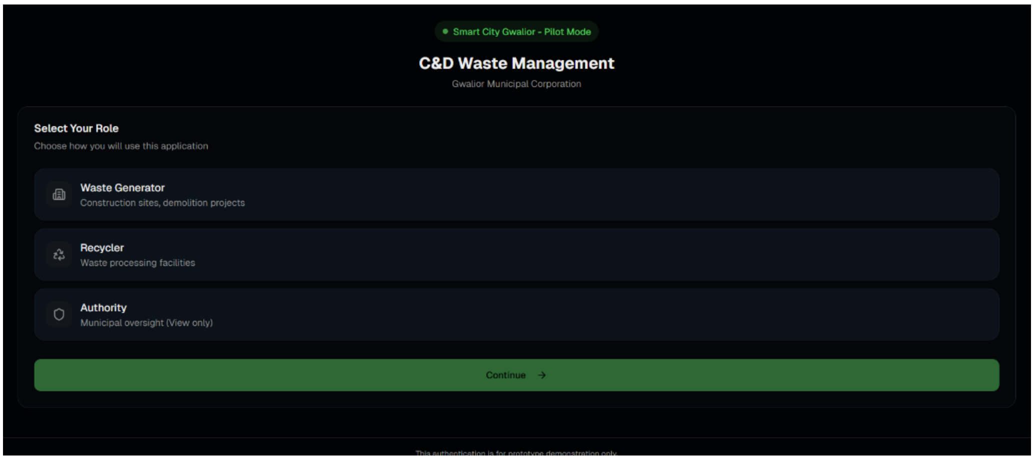

Figure 25. Role-selection interface for Waste Generator, Recycler, and Authority users.

The Waste Generator Dashboard, shown in Figure 26, allows users to track reported waste requests and collection status. The collection workflow is presented through four stages: Submitted, Processing, Scheduled, and Collected. In the displayed dashboard, the request has progressed to the scheduled stage, with collection planned for the following day at 9:00 AM. The vehicle assignment section provides operational details, including vehicle type, driver name, and estimated arrival time (X. Li et al., 2022). This feature improves transparency by allowing waste generators to monitor the movement and status of collection services.

The dashboard also includes an environmental impact section. In the displayed panel, the user has saved 135 kg of CO_2 and submitted 3 reports. The impact analytics indicate 32% reduction in illegal dumping, 18% CO_2 reduction, and 245 litres of fuel saved. Such indicators convert waste-reporting activity into measurable environmental outcomes. The achievement section further supports behavioural engagement through badges such as First Report, Eco Warrior, and Consistent Reporter (L. Akanbi et al., 2020; Qiao et al., 2024).

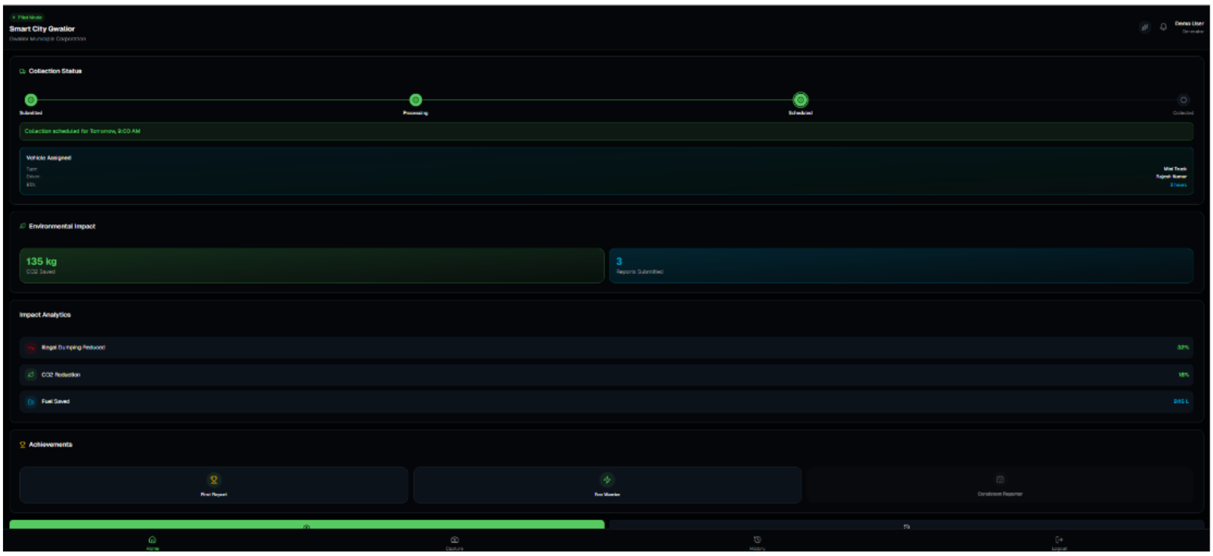

Figure 26. Recycler dashboard module for processing-status monitoring and recycling verification.

The Recycler Dashboard functions as the processing and verification interface for recycling agencies. It enables recyclers to review assigned waste, update processing status, and support verification of whether reported waste has been diverted from disposal pathways to recycling channels. This module acts as the operational bridge between waste generators and municipal authorities. By recording recycler-side updates, the system improves the credibility of waste-management records and reduces dependence on generator-side reporting alone.

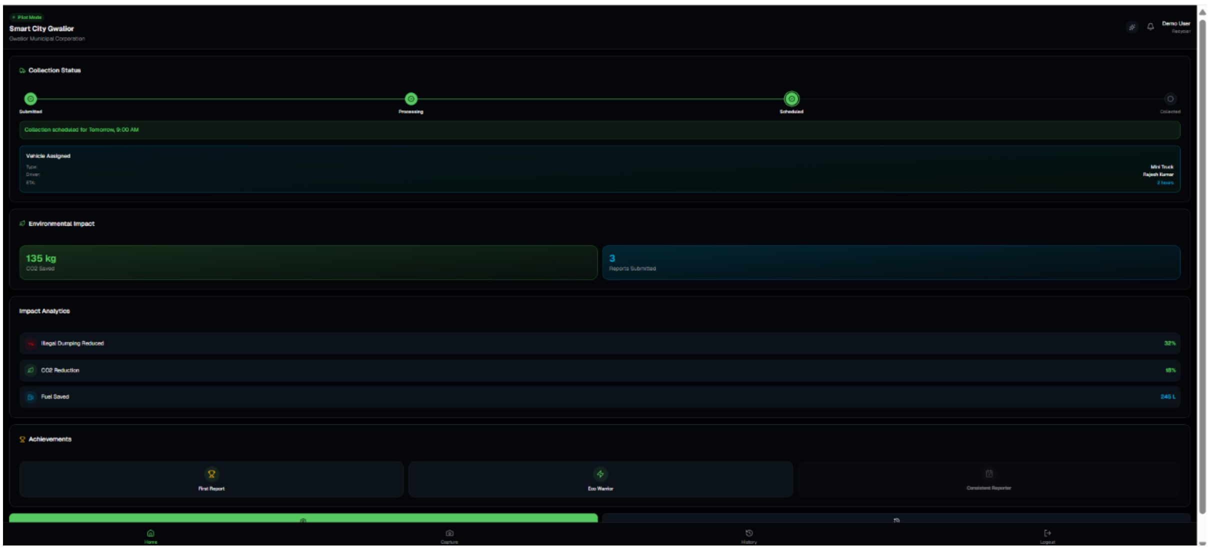

Figure 27. Recycler dashboard module for processing-status monitoring and recycling verification.

The Authority/Admin Dashboard provides a centralized overview of C&D waste management performance across the city. It includes key indicators such as total waste reported, recycled waste, compliance rate, and non-compliance alerts. In the displayed dashboard, the total waste reported is 32.4 tons, of which 22.5 tons has been recycled, indicating an approximate recycling rate of 69%. The compliance rate is shown as 70%, with 7 out of 10 projects following required norms, while 3 non-compliance alerts require administrative attention (Hasibuan et al., 2025; Paz & Lafayette, 2016; Zimmermann et al., 2021). The dashboard also includes trend-based visualizations to compare recycling and landfill disposal over time, helping authorities assess whether recycling performance is improving and landfill dependency is declining.

The report-review module, shown in Figure 28, allows authority users to filter and inspect submitted waste records. The interface includes search and status filters such as All, Submitted, Processing, Scheduled, and Collected. The displayed reports include concrete, mixed, and brick waste entries with their respective volume, weight, location, and status. For example, report NG-2026-001 records concrete waste with a volume of 2.5 m^3 and weight of 450 kg at Lashkar, with status marked as Scheduled. Report NG-2026-002 records mixed waste of 1.8 m^3 and 324 kg at City Center, marked as Collected (Gao et al., 2024; Martins et al., 2026). Report NG-2026-003 records brick waste of 3.2 m^3 and 576 kg at Lashkar, also marked as Collected.

Figure 28. Authority report-review module showing submitted C&D waste records with status filters.

The complete dashboard workflow can be represented as:

Role Selection → Waste Generator / Recycler / Authority Panel
→ Waste Reporting and Tracking → Collection Scheduling
→ Recycling Verification → Authority Monitoring
→ Compliance and Environmental Reporting

Overall, the dashboard extends the proposed AI-based C&D waste analysis framework into a practical municipal decision-support system. While the AI pipeline classifies waste materials, estimates volume, calculates waste mass, and quantifies CO_2 emissions, the dashboard enables these outputs to be reported, monitored, verified, and reviewed through a structured smart-city interface. Therefore, the dashboard serves as the operational layer of the proposed system, supporting stakeholder accountability, transparent collection tracking, recycling verification, compliance control, and environmental performance monitoring for Gwalior Smart City.

5. Conclusion

This study developed an integrated artificial intelligence (AI)-based framework for automated construction and demolition (C&D) waste analysis using manually collected field images from Gwalior Smart City, India. By combining DenseNet121–Transformer classification, LayerCAM-assisted weakly supervised U-Net segmentation, MiDaS-based monocular depth estimation, three-dimensional volume reconstruction, and volume-based CO_2 emission estimation into a unified pipeline, the proposed framework enables comprehensive waste characterization from a single RGB image. The system addresses key limitations of conventional manual inspection by simultaneously identifying waste materials, estimating their spatial extent, quantifying waste volume and mass, and evaluating associated environmental impacts in a fully automated workflow.

Experimental evaluation demonstrated that the proposed classification model achieved an overall accuracy of 87.25%, weighted F1-score of 0.8730, and micro-average AUC of 0.9674, indicating reliable discrimination among the five major C&D waste categories. The weakly supervised segmentation framework attained a validation Dice coefficient of 0.6097 and a mean Intersection-over-Union (IoU) of 0.3396, confirming that LayerCAM-generated pseudo-labels provide an effective alternative to expensive manual pixel-level annotations. Integration of segmentation with monocular depth estimation enabled accurate three-dimensional volume reconstruction directly from smartphone images, eliminating the need for specialized sensing equipment while maintaining practical applicability for field deployment.

The proposed environmental assessment module further demonstrated the capability of AI-driven computer vision to support sustainable waste management. Analysis of the test dataset estimated a total waste volume of 237.87 m^3, corresponding to approximately 582.25 tonnes of waste and 367.45 tonnes of net CO_2 emissions. Steel was identified as the dominant contributor to carbon emissions owing to its high embodied carbon intensity, whereas wood exhibited a carbon-negative contribution because of its sequestration potential. These findings emphasize the importance of material-specific recycling and recovery strategies for reducing the environmental footprint of demolition activities and supporting circular economy initiatives.

Overall, the proposed framework demonstrates that integrating deep learning, weakly supervised segmentation, monocular depth estimation, and environmental analytics provides an effective decision-support system for smart-city C&D waste management. The developed methodology offers significant potential for real-time waste auditing, automated carbon accounting, recycling optimization, and evidence-based urban planning using low-cost smartphone imagery. Future work will focus on expanding the dataset to multiple cities and additional material categories, incorporating instance segmentation and multimodal sensing technologies, improving depth estimation accuracy through multi-view reconstruction, and integrating the framework with cloud-based GIS and Internet of Things (IoT) platforms for continuous city-scale monitoring and intelligent resource management.

References

Aftab, U., Jaleel, F., Aslam, M., Haroon, M., & Mansoor, R. (2024). Building Information Modeling (BIM) Application in Construction Waste Quantification—A Review. In *Engineering Proceedings* (Vol. 75, Issue 1, p. 8). https://doi.org/10.3390/engproc2024075008

Ajayi, S. O., Oyedele, L. O., Bilal, M., Akinade, O. O., Alaka, H. A., Owolabi, H. A., & Kadiri, K. O. (2015). Waste effectiveness of the construction industry: Understanding the impediments and requisites for improvements. *Resources, Conservation and Recycling*, *102*, 101–112. https://doi.org/https://doi.org/10.1016/j.resconrec.2015.06.001

Akanbi, L. A., Oyedele, L. O., Akinade, O. O., Ajayi, A. O., Davila Delgado, M., Bilal, M., & Bello, S. A. (2018). Salvaging building materials in a circular economy: A BIM-based whole-life performance estimator. *Resources, Conservation and Recycling*, *129*, 175–186. https://doi.org/https://doi.org/10.1016/j.resconrec.2017.10.026

Akanbi, L., Oyedele, A., Oyedele, L., & Salami, R. (2020). Deep learning model for Demolition Waste Prediction in a circular economy. *Journal of Cleaner Production*, *274*, 122843. https://doi.org/10.1016/j.jclepro.2020.122843

Akinade, O. O., & Oyedele, L. O. (2019). Integrating construction supply chains within a circular economy: An ANFIS-based waste analytics system (A-WAS). *Journal of Cleaner Production*, *229*, 863–873. https://doi.org/https://doi.org/10.1016/j.jclepro.2019.04.232

Akinade, O. O., Oyedele, L. O., Omoteso, K., Ajayi, S. O., Bilal, M., Owolabi, H. A., Alaka, H. A., Ayris, L., & Henry Looney, J. (2017). BIM-based deconstruction tool: Towards essential functionalities. *International Journal of Sustainable Built Environment*, *6*(1), 260–271. https://doi.org/https://doi.org/10.1016/j.ijsbe.2017.01.002

Araiza-Aguilar, J., Rojas-Valencia, M., Gutierrez, C., Nájera-Aguilar, H., & Gutiérrez, R. (2021). ASSESSMENT OF PHOTOGRAMMETRIC MAPPING TO DETERMINE THE VOLUME OF CONSTRUCTION AND DEMOLITION WASTE. *Environmental Engineering and Management Journal*, *20*, 1087–1097. https://doi.org/10.30638/eemj.2021.101

Cha, G.-W., Moon, H.-J., & Kim, Y.-C. (2021). Comparison of Random Forest and Gradient Boosting Machine Models for Predicting Demolition Waste Based on Small Datasets and Categorical Variables. In *International Journal of Environmental Research and Public Health* (Vol. 18, Issue 16, p. 8530). https://doi.org/10.3390/ijerph18168530

Cha, G.-W., Moon, H. J., & Kim, Y.-C. (2022). A hybrid machine-learning model for predicting the waste generation rate of building demolition projects. *Journal of Cleaner Production*, *375*, 134096. https://doi.org/https://doi.org/10.1016/j.jclepro.2022.134096

Cha, G.-W., Moon, H. J., Kim, Y.-M., Hong, W.-H., Hwang, J.-H., Park, W.-J., & Kim, Y.-C. (2020). Development of a Prediction Model for Demolition Waste Generation Using a Random Forest Algorithm Based on Small DataSets. In *International Journal of Environmental Research and Public Health* (Vol. 17, Issue 19, p. 6997). https://doi.org/10.3390/ijerph17196997

Chen, J., Lu, W., & Xue, F. (2021). "Looking beneath the surface": A visual-physical feature hybrid approach for unattended gauging of construction waste composition. *Journal of Environmental Management*, *286*, 112233. https://doi.org/https://doi.org/10.1016/j.jenvman.2021.112233

Chen, X., Li, Z., Dinesh Peter, J., & Slowik, A. (2023). Circular economy oriented future building information processing: PSO for CNN approach. *Applied Soft Computing*, *149*, 111013. https://doi.org/https://doi.org/10.1016/j.asoc.2023.111013

Cheng, X., Yang, J., Han, Z., Shi, G., Pan, D., Meng, L., Zeng, Z., & Shen, Z. (2024). Optimizing rural waste management: Leveraging high-resolution remote sensing and GIS for efficient collection and routing. *International Journal of Applied Earth Observation and Geoinformation*, *135*, 104219. https://doi.org/https://doi.org/10.1016/j.jag.2024.104219

Davis, P., Aziz, F., Newaz, M. T., Sher, W., & Simon, L. (2021). The classification of construction waste material using a deep convolutional neural network. *Automation in Construction*, *122*, 103481. https://doi.org/https://doi.org/10.1016/j.autcon.2020.103481

Dong, Z., Chen, J., & Lu, W. (2022). Computer vision to recognize construction waste compositions: A novel boundary-aware transformer (BAT) model. *Journal of Environmental Management*, *305*, 114405. https://doi.org/https://doi.org/10.1016/j.jenvman.2021.114405

Etim, E. (2024). Bridging the gap: Transforming waste management awareness into action. *Cleaner Waste Systems*, *9*, 100173. https://doi.org/https://doi.org/10.1016/j.clwas.2024.100173

Gao, Y., Wang, J., & Xu, X. (2024). Machine learning in construction and demolition waste management: Progress, challenges, and future directions. *Automation in Construction*, *162*, 105380. https://doi.org/https://doi.org/10.1016/j.autcon.2024.105380

Hasibuan, G. C. R., Al Fath, M. T., Yusof, N., Dewi, R. A., Syafridon, G. G. A., Jaya, I., Anas, M. R., & Syahrizal. (2025). Integrating circular economy into construction and demolition waste management: A bibliometric review of sustainable engineering practices in the built environment. *Case Studies in Chemical and Environmental Engineering*, *11*, 101159. https://doi.org/https://doi.org/10.1016/j.cscee.2025.101159

Hu, R., Chen, K., Chen, W., Wang, Q., & Luo, H. (2021). Estimation of construction waste generation based on an improved on-site measurement and SVM-based prediction model: A case of commercial buildings in China. *Waste Management*, *126*, 791–799. https://doi.org/https://doi.org/10.1016/j.wasman.2021.04.012

Huang, B., Wang, X., Kua, H., Geng, Y., Bleischwitz, R., & Ren, J. (2018). Construction and demolition waste management in China through the 3R principle. *Resources, Conservation and Recycling*, *129*, 36–44. https://doi.org/https://doi.org/10.1016/j.resconrec.2017.09.029

Huang, L., Cai, T., Zhu, Y., Zhu, Y., Wang, W., & Sun, K. (2020). LSTM-Based Forecasting for Urban Construction Waste Generation. In *Sustainability* (Vol. 12, Issue 20, p. 8555). https://doi.org/10.3390/su12208555

Idir, R., Djerbi, A., & Tazi, N. (2025). Optimising the Circular Economy for Construction and Demolition Waste Management in Europe: Best Practices, Innovations and Regulatory Avenues. In *Sustainability* (Vol. 17, Issue 8, p. 3586). https://doi.org/10.3390/su17083586

Kang, K., Besklubova, S., Dai, Y., & Zhong, R. Y. (2022). Building demolition waste management through smart BIM: A case study in Hong Kong. *Waste Management*, *143*, 69–83. https://doi.org/https://doi.org/10.1016/j.wasman.2022.02.027

Lakhouit, A. (2025). Revolutionizing urban solid waste management with AI and IoT: A review of smart solutions for waste collection, sorting, and recycling. *Results in Engineering*, *25*, 104018. https://doi.org/https://doi.org/10.1016/j.rineng.2025.104018

Lee, D., Kim, S., & Kim, S. (2016). Development of Hybrid Model for Estimating Construction Waste for Multifamily Residential Buildings Using Artificial Neural Networks and Ant Colony Optimization. In *Sustainability* (Vol. 8, Issue 9, p. 870). https://doi.org/10.3390/su8090870

Li, J., Fang, H., Fan, L., Yang, J., Ji, T., & Chen, Q. (2022). RGB-D fusion models for construction and demolition waste detection. *Waste Management*, *139*, 96–104. https://doi.org/https://doi.org/10.1016/j.wasman.2021.12.021

Li, X., Yi, S., Cundy, A. B., & Chen, W. (2022). Sustainable decision-making for contaminated site risk management: A decision tree model using machine learning algorithms. *Journal of Cleaner Production*, *371*, 133612.

https://doi.org/https://doi.org/10.1016/j.jclepro.2022.133612

Lin, K., Zhao, Y., Zhou, T., Gao, X., Zhang, C., Huang, B., & Shi, Q. (2023). Applying machine learning to fine classify construction and demolition waste based on deep residual network and knowledge transfer. *Environment, Development and Sustainability*, *25*(8), 8819–8836. https://doi.org/10.1007/s10668-022-02740-6

Liu, J., Xiao, Y., Wang, D., & Pang, Y. (2019). Optimization of site selection for construction and demolition waste recycling plant using genetic algorithm. *Neural Computing and Applications*, *31*(1), 233–245. https://doi.org/10.1007/s00521-018-3730-8

Lu, W. (2019). Big data analytics to identify illegal construction waste dumping: A Hong Kong study. *Resources, Conservation and Recycling*, *141*, 264–272. https://doi.org/https://doi.org/10.1016/j.resconrec.2018.10.039

Lu, W., Chen, J., & Xue, F. (2022). Using computer vision to recognize composition of construction waste mixtures: A semantic segmentation approach. *Resources, Conservation and Recycling*, *178*, 106022. https://doi.org/https://doi.org/10.1016/j.resconrec.2021.106022

Lu, W., Chen, X., Ho, D., & Wang, H. D. (2015). Analysis of the construction waste management performance in Hong Kong: The public and private sectors compared using big data. *Journal of Cleaner Production*, *112*. https://doi.org/10.1016/j.jclepro.2015.06.106

Lu, W., Long, W., & Yuan, L. (2023). A machine learning regression approach for pre-renovation construction waste auditing. *Journal of Cleaner Production*, *397*, 136596. https://doi.org/https://doi.org/10.1016/j.jclepro.2023.136596

Lu, W., & Tam, V. W. Y. (2013). Construction waste management policies and their effectiveness in Hong Kong: A longitudinal review. *Renewable and Sustainable Energy Reviews*, *23*, 214–223. https://doi.org/https://doi.org/10.1016/j.rser.2013.03.007

Lu, W., & Yuan, H. (2013). Investigating waste reduction potential in the upstream processes of offshore prefabrication construction. *Renewable and Sustainable Energy Reviews*, *28*, 804–811. https://doi.org/https://doi.org/10.1016/j.rser.2013.08.048

Luga, E., Mustafaraj, E., Corradi, M., & Dajko, M. (2025). Recycled red brick masonry demolition waste as a sustainable cement replacement alternative: A DoE-Based approach. *Journal of Building Engineering*, *100*, 111787. https://doi.org/https://doi.org/10.1016/j.jobe.2025.111787

Martins, F. P., Soldal, O. B., Stefanelli, N. O., & Botelho Junior, A. B. (2026). A Scoping

Review of Construction and Demolition Waste Management and the Sustainable Development Goals: Evidence From Brazil. *Sustainable Development*, *34*(S2), 544–555. https://doi.org/https://doi.org/10.1002/sd.70354

Paz, D., & Lafayette, K. (2016). Forecasting of construction and demolition waste in Brazil. *Waste Management & Research*, *34*. https://doi.org/10.1177/0734242X16644680

Qiao, X., Ding, J., She, C., Mao, W., Zhang, A., Feng, B., & Xu, Y. (2024). RETRACTED: A metaheuristic Multi-Objective optimization of energy and environmental performances of a Waste-to-Energy system based on waste gasification using particle swarm optimization. *Energy Conversion and Management*, *317*, 118844. https://doi.org/https://doi.org/10.1016/j.enconman.2024.118844

Shahid, M. U., & Ali, M. (2025). Analyzing barriers to construction waste minimization and circular economy culture in Building projects using fuzzy DEMATEL. *Scientific Reports*, *15*. https://doi.org/10.1038/s41598-025-23188-4

Song, Y., Wang, Y., Liu, F., & Zhang, Y. (2017). Development of a hybrid model to predict construction and demolition waste: China as a case study. *Waste Management*, *59*, 350–361. https://doi.org/https://doi.org/10.1016/j.wasman.2016.10.009

Sosunova, I., & Porras, J. (2022). IoT-Enabled Smart Waste Management Systems for Smart Cities: A Systematic Review. *IEEE Access*, *10*, 1. https://doi.org/10.1109/ACCESS.2022.3188308

Wang, M., Yao, G., Yang, Y., Sun, Y., Yan, M., & Deng, R. (2023). Deep learning-based object detection for visible dust and prevention measures on construction sites. *Developments in the Built Environment*, *16*, 100245. https://doi.org/https://doi.org/10.1016/j.dibe.2023.100245

Zimmermann, R. K., Bruhn, S., & Birgisdóttir, H. (2021). BIM-Based Life Cycle Assessment of Buildings—An Investigation of Industry Practice and Needs. In *Sustainability* (Vol. 13, Issue 10, p. 5455). https://doi.org/10.3390/su13105455

Appendix-I Workshop

As part of the project dissemination and stakeholder engagement activities, a comprehensive **Awareness Program, Dashboard Demonstration, and Python-Based Technical Presentation** was organized at Abhigyan Institute, Tansen Road, Gwalior. The event was designed to educate students and faculty members about sustainable waste management practices while showcasing the technological advancements achieved under the project.

The program provided a platform to demonstrate the developed AI-enabled dashboard, explain the underlying Python-based analytical framework, and highlight the potential of Artificial Intelligence in solving real-world environmental and urban governance challenges.

PROGRAM DETAILS

Event Title

Awareness Program and Technical Demonstration on AI-Based Construction & Demolition Waste Management System

Venue

Abhigyan Institute, Tansen Road, Gwalior

Organizers

- Technology Innovation and Incubation Centre (TIIC), ABV-IIITM Gwalior
- Lord-Tech Datus Solutions Pvt. Ltd.

Participants

Approximately **265 students and faculty members** participated in the event.

Resource Persons

Dr. Kamal Sharma

Principal Investigator and Director, Lord-Tech Datus Solutions Pvt. Ltd.

Dr. Manish Bharadwaj

Co-Investigator

Mr. Prateek Vajpayee

Technical Team Member


AI-Enabled Digital
ABHIGYAAN INSTITUTE


Platform for
Responsible
Management
ABHIGYAAN INSTITUTE

सोना 24 कैरेट 151000
22 कैरेट 139000
चांदी प्रतिकिलो 253000
पेट्रोल 114.76
डीजल 99.85
घरेलू 1025.50
व्यावसायिक 3338.50

सांध्य दैनिक
श्रीराम एक्सप्रेस
सब के साथ

सुविचार
ना तो कोई किसी का मित्र है ना ही शत्रु है। व्यवहार से ही मित्र या शत्रु बनते हैं।
■ हितोपदेश

वर्ष : 17, अंक : 100 | ग्वालियर, गुरुवार 18 जून 2026 | ज्येष्ठ शुक्ल पक्ष 3 (2083) | मूल्य : 3 रु. पृष्ठ : 08

एबीवी-आईआईआईटीएम एवं लॉर्ड-टेक डाटस सॉल्यूशंस विकसित कर रहे एआई आधारित निर्माण एवं ध्वस्तीकरण अपशिष्ट प्रबंधन तंत्र

श्रीराम एक्सप्रेस। ग्वालियर

ग्वालियर स्मार्ट सिटी के लिए तैयार हो रहा अत्याधुनिक एआई डैशबोर्ड, 400 विद्यार्थियों को दी परियोजना की जानकारी।

ग्वालियर। अटल बिहारी वाजपेयी भारतीय सूचना प्रौद्योगिकी एवं प्रबंधन संस्थान (एबीवी-आईआईआईटीएम), ग्वालियर के प्रौद्योगिकी नवाचार एवं उद्भवन केंद्र (टीआईआईसी) तथा लॉर्ड-टेक डाटस सॉल्यूशंस प्राइवेट लिमिटेड के सहयोग से 'ग्वालियर स्मार्ट सिटी के लिए कृत्रिम बुद्धिमत्ता (एआई) आधारित निर्माण एवं ध्वस्तीकरण अपशिष्ट प्रबंधन तंत्र' विकसित किया जा रहा है। इस परियोजना के अंतर्गत एक अत्याधुनिक एआई डैशबोर्ड तैयार किया जा रहा है, जो निर्माण एवं ध्वस्तीकरण अपशिष्ट की मात्रा और उसकी संरचना का सटीक आकलन करने में सक्षम होगा।

परियोजना का उद्देश्य निर्माण गतिविधियों से उत्पन्न अपशिष्ट के वैज्ञानिक प्रबंधन, पुनर्चक्रण तथा संसाधनों के सतत उपयोग को बढ़ावा देना है। विकसित की जा रही प्रणाली कंक्रीट, ईंट, इस्पात, लकड़ी, कांच सहित विभिन्न निर्माण सामग्रियों से उत्पन्न अपशिष्ट का अनुमान लगाकर उनके प्रभावी प्रबंधन और पुनर्चक्रण के लिए उपयोगी आंकड़े उपलब्ध कराएगी।

परियोजना में लॉर्ड-टेक डाटस सॉल्यूशंस प्राइवेट लिमिटेड के निदेशक डॉ. कमल शर्मा प्रधान अन्वेषक के रूप में कार्य कर रहे हैं, जबकि मनीष भारद्वाज और अमल वाजपेयी सह-अन्वेषक हैं। तकनीकी विकास एवं क्रियान्वयन में राजुल जैन, धर्मेन्द्र प्रजापति और प्रतीक वाजपेयी महत्वपूर्ण भूमिका निभा रहे हैं।

परियोजना के अंतर्गत तानसेन रोड स्थित अभिज्ञान इंस्टीट्यूट में जन-जागरूकता एवं प्रसार कार्यक्रम आयोजित किया गया, जिसमें लगभग 400 विद्यार्थियों और शिक्षकों ने सहभागिता की। इस अवसर पर डॉ. कमल शर्मा,

मनीष भारद्वाज और प्रतीक वाजपेयी ने परियोजना की अवधारणा, कार्यप्रणाली, उपयोगिता तथा पर्यावरणीय लाभों पर विस्तृत जानकारी दी।

कार्यक्रम में प्रतिभागियों को निर्माण एवं ध्वस्तीकरण अपशिष्ट प्रबंधन की चुनौतियों, पुनर्चक्रण की संभावनाओं तथा एआई आधारित समाधानों के महत्व से अवगत कराया गया। विद्यार्थियों और शिक्षकों ने इस पहल को स्मार्ट सिटी विकास, स्वच्छता प्रबंधन, संसाधन संरक्षण और पर्यावरणीय स्थिरता की दिशा में महत्वपूर्ण कदम बताया।

परियोजना को एबीवी-आईआईआईटीएम ग्वालियर के प्रोफेसर डॉ. मनोज पटवर्धन का सतत मार्गदर्शन प्राप्त हो रहा है। उनके निर्देशन में पायलट परियोजना निरंतर प्रगति पर है और अपशिष्ट प्रबंधन के लिए तकनीक आधारित नवाचारी समाधान विकसित किए जा रहे हैं।

डॉ. कमल शर्मा ने बताया कि यह एआई डैशबोर्ड भविष्य में नगर निगमों, निर्माण एजेंसियों और नीति-निर्माताओं को डेटा-आधारित निर्णय लेने में सहायता प्रदान करेगा। वर्तमान में परियोजना का पायलट चरण संचालित है तथा प्राप्त परिणामों के आधार पर इसके व्यापक उपयोग की संभावनाओं पर कार्य किया जा रहा है।